MINNESOTA GEOLOGICAL SURVEY
Harvey Thorleifson, *Director*

CHARACTERIZATION OF THE PHILBROOK INTRUSION, CENTRAL MINNESOTA

Terrence J. Boerboom
Minnesota Geological Survey

Jesse Geary
Macalester College

Report of Investigations 71
ISSN 0076-9177

UNIVERSITY OF MINNESOTA
Saint Paul — 2017

CHARACTERIZATION OF THE PHILBROOK INTRUSION, CENTRAL MINNESOTA

This publication is accessible from the home page of the Minnesota Geological Survey (http://www.mngs.umn.edu) as a PDF file readable with Acrobat Reader 5.0.

Date of release: May, 2017

Recommended citation
Boerboom, T.J., and Geary, J., 2017, Characterization of the Philbrook intrusion, central Minnesota: Minnesota Geological Survey Report of Investigations 71, 20 p.

Minnesota Geological Survey
2609 Territorial Road
Saint Paul, Minnesota 55114

Telephone: 612-626-2969
E-mail address: mgs@umn.edu
Web site: http://www.mngs.umn.edu

ISSN 0076-9177

CONTENTS

FIGURES

TABLES

NOTE ON MEASUREMENTS USED IN THIS REPORT

Although the metric system is preferred in scientific writing, certain measurements are still routinely made in English customary units; for example, distances on land are measured in miles and depths in drill holes are measured in feet. Preference was given in this report to retaining the units in which measurements were made. To assist readers, conversion factors for some of the common units of measure are provided below.

English units to metric units:

To convert from	to	multiply by
inch	millimeter	25.40
inch	centimeter	2.540
foot	meter	0.3048
mile	kilometer	1.6093

Metric units to English units:

To convert from	to	multiply by
millimeter	inch	0.03937
centimeter	inch	0.3937
meter	foot	3.2808
kilometer	mile	0.6214

CHARACTERIZATION OF THE PHILBROOK INTRUSION, CENTRAL MINNESOTA

Terrence J. Boerboom and Jesse Geary

ABSTRACT

The Philbrook intrusion is an informal name for a small, sub-circular mafic pluton that is exposed at the surface along the southeast side of the Long Prairie River near the town of Philbrook, in northeastern Todd County, central Minnesota. An $^{40}Ar/^{39}Ar$ age of 1,854 ± 4 Ma has been obtained from a sample of what is interpreted to be magmatic hornblende from the intrusion. The pluton is composed primarily of melanocratic to mesocratic diorite, along with substantial proportions of pyroxenite, hornblendite, oxide-apatite rock (nelsonite), and rare anorthosite as inclusions in the mesocratic diorite. The Philbrook intrusion contains abundant hornblende interpreted to be both primary-magmatic and secondary-deuteric, which coupled with local net-veined pegmatitic textures and pervasively saussuritized plagioclase, imply that the magma was rich in hydrous components. Even though primary textures are commonly overprinted by secondary hornblende, relict primary cumulate textures are present in most of the different rock types. Chemically, the entire suite of rocks is high in phosphorous, iron, titanium, and vanadium, and low in silica, magnesium, and potassium.

Due to the high content of Fe-Ti oxide minerals, the Philbrook intrusion produces a pronounced positive magnetic anomaly. This anomaly was identified by early dip-needle surveys that led to the drilling of 12 exploratory holes between approximately 65 and 250 feet (20 and 76 meters) in depth, in the early 1900s by Adams Exploration, presumably for iron ore. Although the results of this drilling apparently did not lead to a deposit deemed economic, the elevated iron, titanium, and vanadium values, especially in the oxide-rich phases, may be of future economic interest. Apatite, which is abundant, does not contain any substantial rare-earth element concentrations, and does not warrant economic interest.

The Philbrook intrusion was emplaced into a suite of interlayered sedimentary, volcanic, and hypabyssal intrusive rocks that have been inferred to be Paleoproterozoic, but have more recently been interpreted to be possibly Archean, in age. The country rocks are schistose and were regionally metamorphosed to the upper greenschist/lower amphibolite facies, either during or before the Penokean Orogeny, or possibly both, depending on their age, which is unknown.

Based on available drill cores and outcrops, the intrusion is largely undeformed, but is locally transected by northwest-trending shear zones, and the margins of the intrusion contain a weak penetrative cleavage. The 1,854 ± 4 Ma age is very similar to metamorphic ages obtained from the Cuyuna North Range and from the Mille Lacs Group, within the Penokean Orogen to the east of this body, and it cannot be ruled out that this date actually reflects resetting by this widespread Penokean metamorphic event. However, assuming this is a magmatic age, the Philbrook intrusion was emplaced during the Penokean Orogeny, which peaked around approximately 1,870 Ma and ended at approximately 1,830 Ma.

INTRODUCTION

The Philbrook intrusion is inferred to be a funnel- or plug-shaped, 1.5-mile-diameter (2.4-kilometer) pluton composed of a suite of rocks with atypically high concentrations of iron, titanium, and phosphorus. These include diorite, hornblendite, hornblende pyroxenite, oxide-apatite rock (nelsonite), and minor anorthosite; all except the anorthosite contain anomalously high concentrations of Fe-Ti oxides and apatite. Apatite is most abundant in the melanocratic diorite phases, although anomalous concentrations are also present in the other rock types.

The pluton intrudes stratified supracrustal rocks, which had been interpreted to be Paleoproterozoic (Southwick and others, 1988), but more recently have been ambiguously interpreted to be Archean, in age (Fig. 1; Jirsa and others, 2011). The intrusion is well-defined by a sharp, positive aeromagnetic anomaly (Fig. 2), and it is exposed in a series of low outcrops in northeastern Todd County adjacent to the town of Philbrook near the Long Prairie River. In addition to the surface exposures, several drill

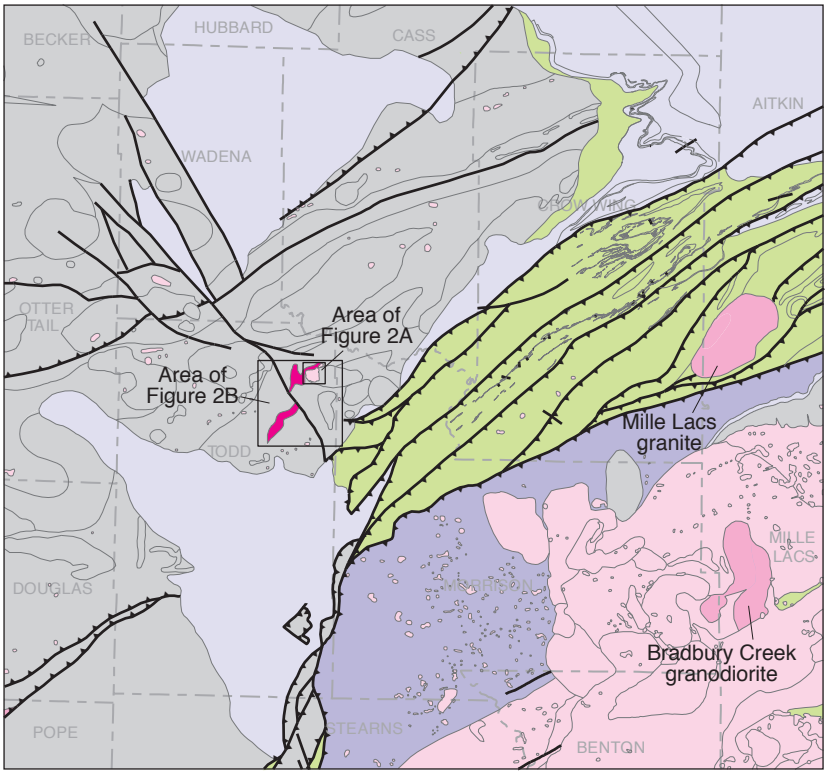

Figure 1. Simplified geologic bedrock map of east-central Minnesota showing the location of the Philbrook intrusion (within area of Fig. 2A and designated by a star on the inset map). Regional map modified from Jirsa and others (2011).

INDEX

Paleoproterozoic

- Animikie basin and outliers (dominantly low-grade graywacke-slate sequences)
- Rocks of the Penokean Orogen, undivided
- Little Falls Formation (staurolite-garnet schist; metagraywacke)
- East-central Minnesota batholith and Penokean intrusions
- Penokean intrusive rocks

Paleoproterozoic to Archean

- Philbrook and Fawn Lake iron formation and associated rocks

Archean

- Archean bedrock, undivided

- Fault
- Thrust fault

cores are available from the southern part of the pluton (Fig. 2). Mesocratic to melanocratic diorite/altered gabbro dominate in the outcrops, whereas pyroxenite, hornblendite, and oxide rock make up most of the drill cores; however, the cores have been skeletonized, rending uncertainty to the relative proportions of the various rock types. Outcrop data and drill core stratigraphy combined with aeromagnetic data imply that overall the diorite phases are predominant, whereas the other rock types form possibly concentric but apparently irregular internal layers or segregations (Fig. 2).

HISTORY OF INVESTIGATIONS

Previous investigations of the Philbrook intrusion have been cursory. The outcrops were first noted as "…dark and tough, nearly black dioryte…" that "… ring[s] sonorously like an iron kettle when struck by a hammer" (Upham, 1888, p. 568). In the early 1900s, twelve drill holes were placed over a magnetic, oxide-rich portion of the intrusion by Cuyler Adams in a search for iron ore. Subsequent to drilling, the drill cores were reduced to short 2- to 4-inch (5- to 10-centimeter) pieces representative of 10-foot (3-meter) intervals and preserved in small, labeled glass bottles. These were donated to the Minnesota Geological Survey and are now stored at the Minnesota Department of Natural Resources drill core library in Hibbing, Minnesota. How the cores were skeletonized is unknown and it can only be assumed that the preserved core is representative of the core intervals.

Thiel (1926) and Grout and Wolff (1955) briefly mentioned the outcrops, and a ground magnetic and gravity study of the pluton was conducted by Cade (1987). Two 10-foot (3-meter) drill cores were obtained by the Minnesota Geological Survey as part of a regional scientific bedrock-drilling program (Southwick and others, 1990). Outcrop mapping was completed in the early 1980s as part of an M.S. thesis by Boerboom (1987), and many more details of the pluton and surrounding rocks can be found in that publication. The Philbrook area is also included in the Todd County Geologic Atlas, which incorporated the earlier studies (Boerboom, 2007).

Boerboom (1987) only briefly examined the outcrops during his original mapping, and now detailed lidar data that were not available at that time could help accurately locate all the outcrops, which may lead to reinterpretation of the intrusion. For this study, the remains of the original drill cores were thoroughly examined. Approximately 25 thin sections of the intrusion were examined, and 5 polished plugs were made from samples of the oxide rocks and hornblendites/pyroxenites. Several of the thin sections were also polished for reflective microscopy and electron microprobe analyses. Representative samples from each of the major rock types were point-counted with a minimum of 1,000 points per thin section. Visual estimates were made on rock types that were too coarse-grained to accurately point count.

Geary (2012) sampled several of the diorite outcrops for geochemical analyses as part of a senior thesis at Macalester College; those analyses are included in this report.

AGE AND GEOLOGIC SETTING

The contact between the Philbrook pluton and the country rock is not exposed; however, it presumably intrudes a sequence of schistose, heterolithic, conglomeratic rocks (unit APs on Fig. 2A) that are exposed in a series of outcrops within 250 feet (76 meters) of the northernmost exposure of the Philbrook pluton. Based on cursory investigation, the conglomerate contains clasts of quartz-rich sedimentary rocks, hypabyssal tonalite, and possible volcanic rocks. Another nearby outcrop is composed of massive, foliated, porphyritic hypabyssal biotite tonalite; however, the relationships to the conglomerate are not known. The conglomerate does not contain clasts from the Philbrook intrusion, but rather has been recrystallized by possible contact metamorphism and metasomatic alteration from it (Boerboom, 1987). This conglomerate has been inferred to comprise the basal part of the Paleoproterozoic Mille Lacs Group resting directly on Archean crust (Southwick and others, 1988), but subsequent investigators have raised the possibility that this sequence could be Archean in age, as described below.

In addition to the drill holes in the Philbrook intrusion, several other core holes that date from the early 1900s were drilled approximately 1 mile (1.6 kilometers) west of the pluton (Figs. 1, 2B). This drilling delineated the Philbrook iron formation—a reserve of north–south striking, steeply east-dipping magnetite and hematite iron ore intercalated with chlorite schist and albite-rich, possibly hydrothermally-altered metasedimentary rocks, as well as metamorphosed mafic volcanic or hypabyssal intrusive rocks (Boerboom, 1987, 1989, 2007). The Philbrook iron formation produces a prominent positive aeromagnetic anomaly that is of similar orientation and amplitude to a magnetic anomaly produced by the Fawn Lake iron formation to the south, and the two iron-formation bearing

A.

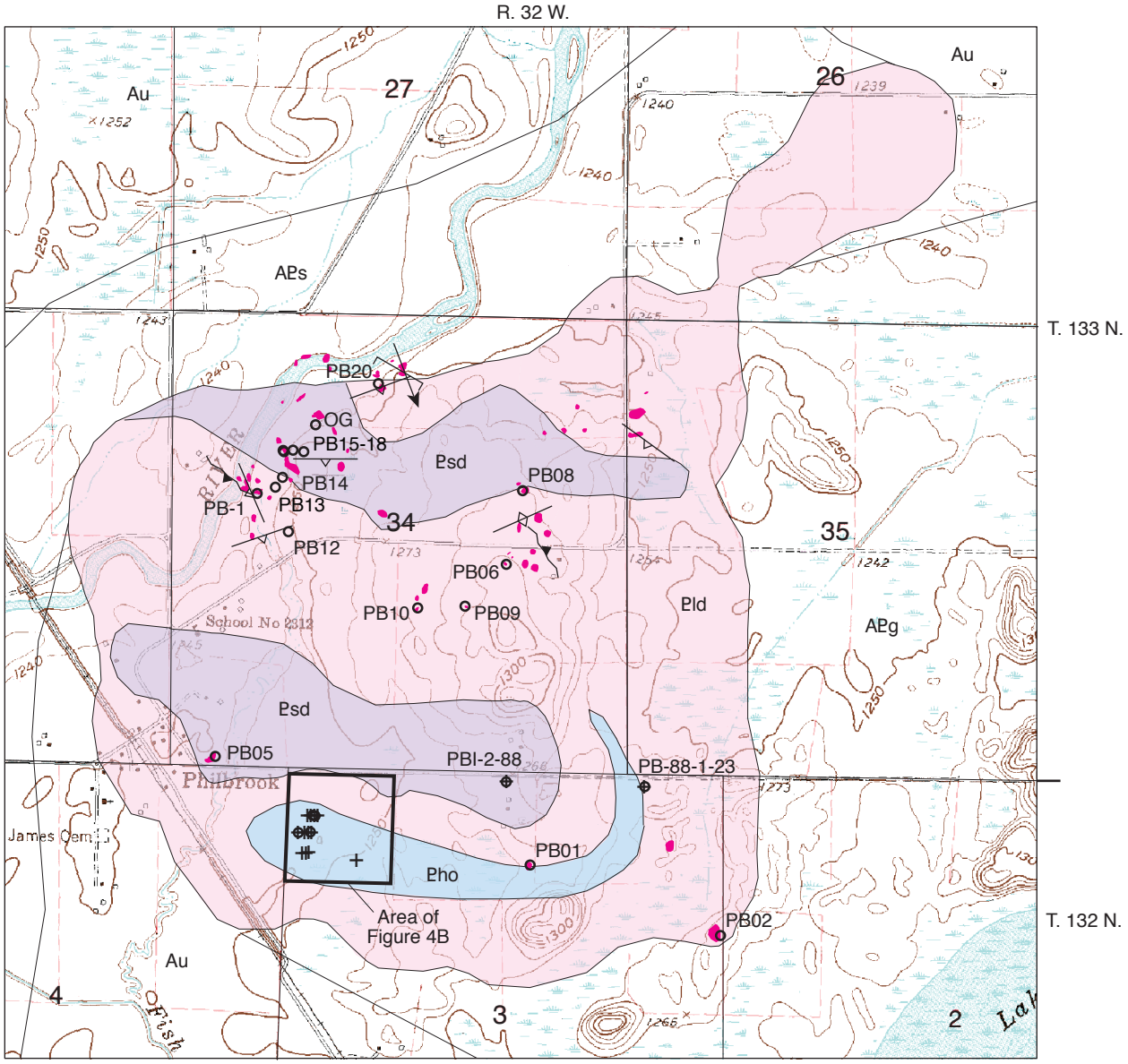

INDEX

- + Location of drill hole with available core
- Outcrop
- Location of geochemical sample
- Strike and dip (unspecified angle) of fabric in narrow shear bands
- Strike and dip (unspecified angle) of igneous foliation or layering
- Strike and dip of metamorphic foliation in metasedimentary rocks
- Lineation of stretched clasts in metaconglomerate

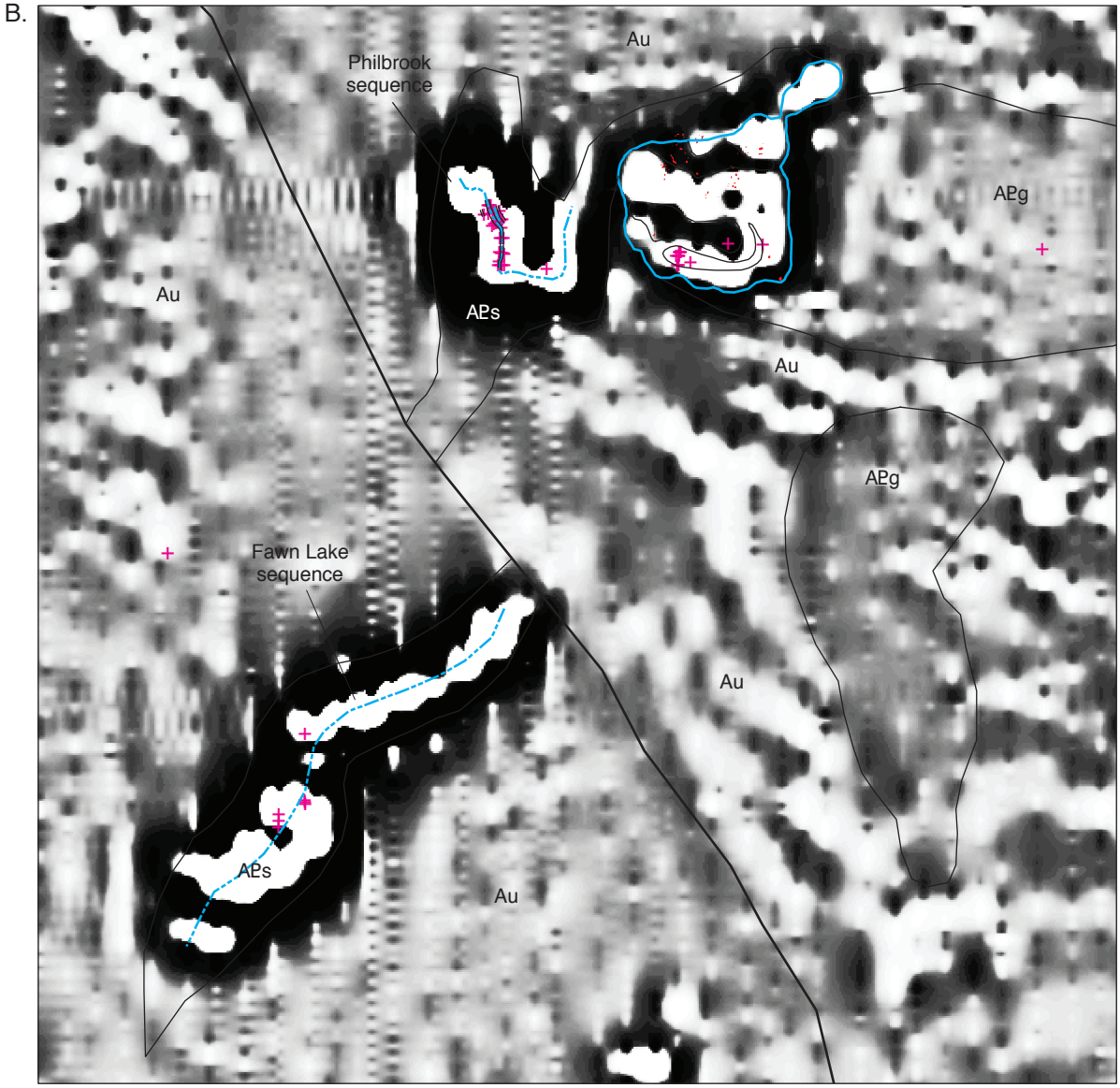

Figure 2. A. Bedrock geologic map of the Philbrook intrusion and environs. Pld—Melanocratic diorite; Psd—Mesocratic diorite; Pho—Pyroxenite, hornblendite, and oxide-apatite rock; APg—Archean or Paleoproterozoic granite; APs—Archean and/or Paleoproterozoic metasedimentary rocks including metamorphosed iron formation (shown by blue dashed line on Fig. 2B) and conglomerate, also fine-grained clastic metasedimentary rocks and minor metadiorite; Au—Archean rocks, undivided. Location shown on Figure 1. Geology modified from Boerboom (1987, 2007) and Jirsa and others (2011).

B. First-vertical derivative aeromagnetic anomaly map of the Philbrook intrusion (outlined in blue) and the Philbrook iron formation (strong positive anomaly west of the Philbrook intrusion). Locations of the drill holes are shown by crosses. Location shown on Figure 1.

sequences are interpreted to be continuous but offset by a major northwest-trending fault (Figs. 1, 2B; Boerboom, 2007; Jirsa and others, 2011). Skeletonized drill core from the Fawn Lake iron formation shows that it is associated with metamorphosed gabbro to quartz diorite and altered supracrustal rocks, which are intruded by dikelets of deformed granite. These iron formations and associated rocks were depicted as forming the western extension of the Paleoproterozoic Mille Lacs Group by Southwick and others (1988), but based on the metamorphosed and deformed character of both the Philbrook and Fawn Lake sequences, they may alternatively be Archean in age (Jirsa and others, 2011).

Hornblende from the Philbrook pluton, interpreted to be mainly magmatic but possibly in part deuteric after earlier clinopyroxene, yielded an $^{40}Ar/^{39}Ar$ age of 1,854 ± 4 Ma, a minimum age that dates the time at which the pluton cooled below the blocking temperature of hornblende (Southwick, 1994). Although the intrusion lacks a pervasive regional metamorphic foliation, it is transected by several northwest-striking brittle to ductile fractures and shear bands. Some of the ductile deformation bands contain relatively coarse-grained neomorphic actinolitic hornblende; others are comprised of fine-grained, chlorite-actinolite schist. The recrystallized nature of the amphibole in these bands implies that at least some of the deformation involved shearing and recrystallization under high-temperature hydrous conditions; however, the round shape of the pluton and the general lack of regional deformation fabrics within it indicate that emplacement was syn- to post-tectonic relative to deformation of the surrounding rocks. This is consistent with the inference that the Penokean Orogeny had culminated by 1,870 Ma (Southwick and others, 1988) and ended by 1,830 Ma (Schulz and Cannon, 2007).

If 1,854 Ma is an emplacement age, then it is close in timing to the Bradbury Creek granodiorite (Fig. 1), which yielded U-Pb zircon ages between 1,858 ± 11 and 1,877 ± 15 Ma (Holm and others, 2005). A slightly older granitic intrusion (the Mille Lacs granite; 2,009 ± 7 Ma; Fig. 1; Holm and others, 2005), located within the heart of the Penokean Orogen and emplaced into the Mille Lacs Group, predates the age obtained on the Philbrook intrusion, implying that scattered plutonism was taking place within the Penokean Orogen as it was forming. Because the 1,854 Ma age on the Philbrook intrusion represents a minimum age that marks the temperature for blocking the release of argon from hornblende, the actual time of emplacement may overlap with the Bradbury Creek granodiorite or the Mille Lacs granite.

Alternatively, in situ U-Pb microgeochronologic studies of hydrothermal or diagenetic xenotime and metamorphic monazite, from supracrustal rocks located within the Penokean Orogen east of Philbrook, have documented metamorphic and hydrothermal events related to both the Penokean (approximately 1,860 Ma) and Yavapai (approximately 1,760 Ma) Orogens (for example Schneider and others, 2004; Holm and others, 2007; Vallini and others, 2007). Although petrographic and compositional data (Boerboom, 1987; Southwick, 1994) support a magmatic origin for the hornblende samples used for geochronologic study of the Philbrook intrusion, it cannot be ruled out that the 1,854 Ma age records a Penokean metamorphic overprint similar to that identified in the adjacent Penokean orogenic belt.

Regardless of whether the 1,854 Ma age on the Philbrook intrusion is a proxy for the time of emplacement, or represents a metamorphic reset event, it is clearly older than the multiple components of the east-central Minnesota batholith, which range in age from 1,772 to 1,800 Ma, an age range that corresponds to the Yavapai orogeny (Fig. 1; Holm and others, 2005). Although several of the individual intrusions that comprise the east-central Minnesota batholith have characteristics that imply they could also be related to massif anorthosites (for example charnockitic granite, noritic anorthosite, rapakivi-textures; Boerboom and others, 1995; Boerboom and Holm, 2000), the Philbrook intrusion is clearly older by at least 50 million years, and thus likely is not related to that large, intrusive complex.

PETROGRAPHY

The IUGS classification scheme of Streckeisen (1973; Fig. 3) is used to classify rocks with less than 80 percent opaque Fe-Ti-oxide minerals. Those containing greater than 80 percent oxides are termed oxide rock, or nelsonite if they contain substantial apatite (Watson and Taber, 1913). The term hornblendite is used for all amphibole-rich (greater than 90 percent) rocks, even though much of the amphibole consists of secondary hornblende and actinolite. As described below, these secondary amphiboles are inferred to have formed by late-stage magmatic-deuteric alteration, rather than regional metamorphism, and thus are considered igneous in origin (hence the term hornblendite instead of the metamorphic term amphibolite). Modal analyses of representative rock types are listed in Table 1, and geochemical analyses of various units are listed in Table 2. Drill core logs and cross sections of the drill holes are portrayed in Figure 4.

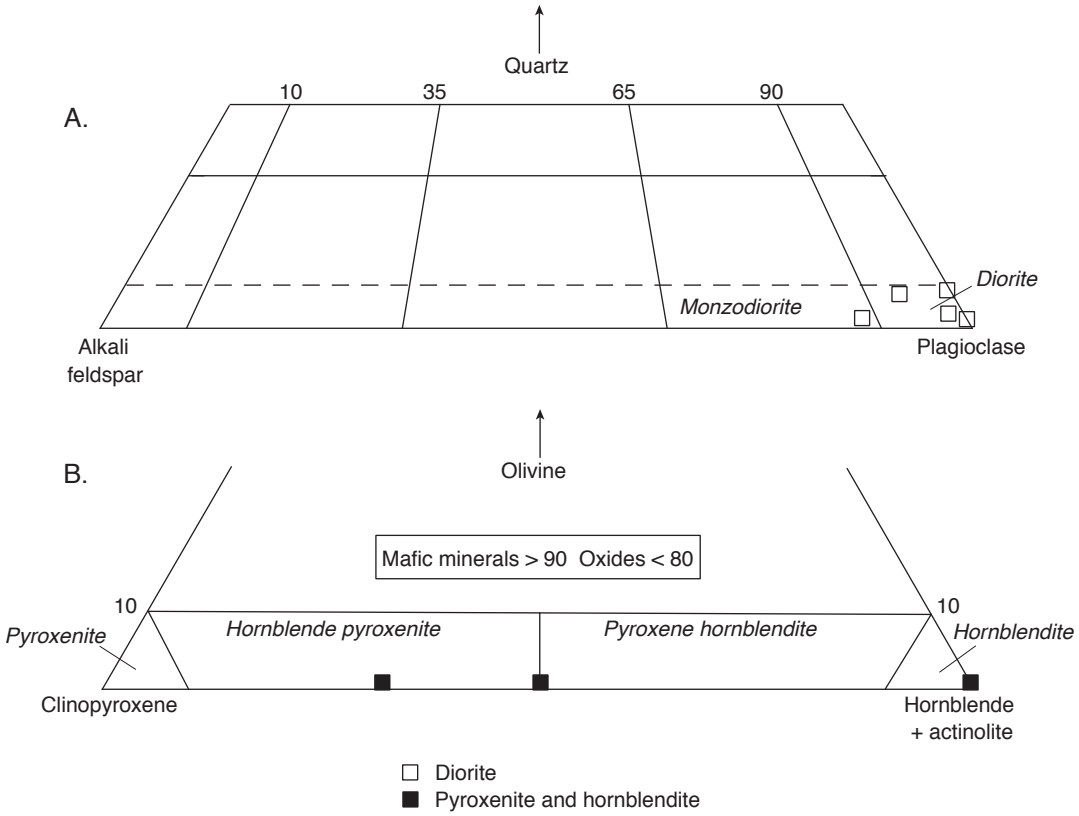

Figure 3. Igneous rock classification diagrams for samples of the Philbrook intrusion. Oxide rock and nelsonite are not shown. Modified from Streckeisen (1973).

Diorite

The bulk of the outcrops and a minor proportion of the drill cores consist of dark green melanocratic diorite (meladiorite) or greenish-white mesocratic diorite (mesodiorite), which are described separately below. The mesodiorite contains local inclusions of anorthosite, and thin amphibole veinlets are common throughout both diorite phases.

Melanocratic diorite

Dark green, medium-grained, high P-Fe-Ti meladiorite contains abundant deuteric hornblende and actinolite that have variably replaced pyroxene and plagioclase; where alteration is complete the meladiorite locally grades into hornblendite. Cumulus textures and modal layering are characteristic, the former defined by aligned plagioclase, apatite, and rectangular mafic minerals (Fig. 5) and the latter by 1- to 3-inch (2- to 8-centimeter) thick leucocratic layers alternating with 6- to 12-inch (15- to 30-centimeter) thick hornblende-rich melanocratic layers. Although modal layering is difficult to observe in outcrop, it is well demonstrated in nearby boulders (Fig. 6).

Several 2- to 39-inch (5- to 100-centimeter) wide, strongly foliated, north–northwest trending, subvertical protomylonitic shear zones were noted in outcrops of meladiorite. These shear zones contain rolled feldspar porphyroclasts less than 2 millimeters in diameter surrounded by pressure shadows of quartz, chlorite, and amphibole (Fig. 7), and trains of broken ilmenite rods formed by the cataclasis of skeletal ilmenite are common, as are thin foliation-parallel quartz-carbonate veinlets.

The mineralogy of the meladiorite is dominated by various primary and secondary amphiboles, andesine, augite, Fe-Ti oxides, and apatite (Table 1), as well as possible olivine pseudomorphs (Fig. 5) that consist of granular to skeletal-habit oxide minerals surrounded by ferromagnesian silicate minerals (Fig. 8).

Andesine (An_{40-52}; Table 3) forms tabular crystals variably altered to sericite, preferentially in cores, and granular epidote, which is evenly distributed throughout the crystals. Microprobe analyses show no chemical variation from cores to rims, despite a weak optical zonation, implying reequilibration by

Table 1. Modal analyses of some representative rock types from the Philbrook pluton.

Rock type	Melanocratic diorite			Mesocratic diorite			Hornblende pyroxenite	Hornblendite
Sample	PB-1	3A	1A-4[3]	OG	10	11-6	D1-74[3]	D3-150[3]
Hornblende[1]	19	u	u	12	14	10	15	T
Actinolite[1]	32	u	u	10	14	15	5	76
Amphibole[2]	51	59	22	22	28	25	20	76
Pyroxene	-	3	15	4	-	-	44	-
Opaque oxides	10	7	8	4	5	4	17	35
Andesine	29	22	44	57	39	60	-	-
Albite	T	-	T	5	6	1	-	-
Apatite	5	6	8	4	1	T	T	6
Chlorite	T	T	-	-	5	2	1	T
Biotite	4	-	3	3	5	2	-	T
Calcite	-	-	-	T	-	-	T	-
Quartz	-	-	-	2	T	-	-	-
Epidote	T	-	-	T	11	5	-	-
Sphene	-	-	-	-	-	-	T	-
Sulfide minerals	-	-	-	-	-	-	-	T
Iddingsite	-	-	T	-	-	-	-	-

REFLECTED LIGHT

Rock type	Melanocratic diorite			Mesocratic diorite
Sample	D1-52	D3-150	D12-60	D8-55
Magnetite	44	18	T	T
Exsolved ilmenite	34	15	1	3
Composite ilmenite	8	4	9	6
Hematite	2	T	-	-
Sulfide minerals	T	1	T	1
Other (silicates)	12	62	90	90

[1]Actinolite is difficult to distinguish from hornblende, and the relative proportions are estimates.
[2]Sum of all amphiboles with no distinction between various types.
[3]Estimate, not point counted.

Samples from outcrop:

PB-1	T. 133 N., R. 32 W., sec. 34, BCDBD
3A	T. 133 N., R. 32 W., sec. 34, BCDBD
1A-4	T. 133 N., R. 32 W., sec. 35, BCBBB
OG	T. 133 N., R. 32 W., sec. 34, BACDC
10	T. 133 N., R. 32 W., sec. 34, BDABC
11-6	T. 133 N., R. 32 W., sec. 34, CCCDC

Samples with a "D" prefix are from drill core; for example, D1-52 = drill hole 1 at 52 feet depth. See Figure 2 for location of drill holes.

- = No detection T = Trace amount u = Undifferentiated amphibole

deuteric processes. Most plagioclase is stained by fine-grained microscopic iron-oxide dust. Grain boundaries are ragged due to peripheral penetration by secondary prismatic hornblende, and in some cases this replacement is pervasive (Fig. 5). Albite in trace amounts (Table 3) forms anhedral-interstitial grains that contain fine-grained, wispy, prismatic actinolite. Although the albite shows an antiperthitic texture under the microscope, microprobe analyses show no appreciable potassium. Rare myrmekitic quartz/feldspar intergrowths separate andesine and albite.

Iron and calcium-rich augite (Table 4, samples PX2-OG and PX3-OG) forms light brown, prismatic,

cumulate to subophitic grains; however, most augite has been replaced by pseudomorphs of pale green, fibrous uralitic amphibole (Fig. 5). All of the augite that is still recognizable exhibits a prominent herringbone texture formed by fibrous actinolite, which may be secondary after original exsolution lamellae of calcium-poor orthopyroxene. Small inclusions of rounded plagioclase, prismatic apatite, and fine-grained, dusty, opaque oxides of secondary origin are common.

A variety of amphibole types occur within the meladiorite, but there are two main types: 1. Fibrous, light green actinolite that has replaced pyroxene, and 2. Deep blue-green ferropargasitic hornblende that forms prismatic rims around relict pyroxene grains, and that typically penetrate into adjacent plagioclase (Fig. 5).

The fibrous pseudomorphic actinolitic amphiboles (type 1) form green fibrous mats that replace pyroxene and possibly earlier magmatic hornblende, and are mixed with varied proportions of tiny opaque oxides and sphene or leucoxene. The degree of replacement varies from incipient alteration that mimics relict herringbone structures in augite, to pale green to colorless felty mats that completely overprint augite (Fig. 5).

The prismatic pargasitic hornblende (type 2) may be the product of a deuteric reaction between primary augite and plagioclase (Fig. 5). Plagioclase locally may be completely obliterated by this type of amphibole, as evidenced by zones of plagioclase that are in optical continuity but contained with mats of this amphibole type. It is chemically similar to the red-brown magmatic hornblende in the pyroxenite/hornblendite (discussed below) except for slightly higher aluminum content. Scraps of brown biotite and opaque oxides are commonly associated with this type.

Minor proportions of subpoikilitic, apparently magmatic, ferropargasitic hornblende (Table 5A; samples HB-35-1 and HB-36-1), which is choked with dark brown rods of rutile and cleavage-fracture controlled secondary opaque oxides, is commonly associated with dark red-brown biotite that is in optical continuity.

Most biotite occurs as a late metasomatic alteration product of magnetite that originally contained exsolution lamellae of ilmenite. Complete replacement results in clots of biotite, which contain relict ilmentite lamellae, to Fe-Ti oxide (ilmenomagnetite) grains rimmed by biotite, in some cases with blades of exsolved ilmenite projecting out of the unaltered oxide grains into the rimming biotite. Lesser amounts of chlorite and amphibole have also replaced the original magnetite in the same manner as biotite. This occurrence is similar to that described by Morse (1979) in the Kiglapait intrusion, where biotite is ascribed to a crystal-liquid reaction that correlates with the abundance of oxide minerals and with increased concentration of fluorine (corresponding with apatite) in the liquid. The chemical composition of biotite is summarized in Table 6.

Ilmenite is the predominant oxide mineral and ranges from discrete interstitial blebs to skeletal crystals intergrown with chlorite, biotite, or amphibole as previously described. Some concentrations of fine granular oxides (most likely magnetite) may be pseudomorphic after primary olivine.

Apatite comprises 8 to 20 percent of the rock, mainly as euhedral, 1 to 3 millimeter, prismatic grains that define a weak cumulate foliation (Fig. 5). Locally, poikilitic apatite crystals as much as 6 millimeters in diameter enclose feldspar and hornblende. Apatite inclusions within hornblende, pyroxene, and plagioclase become larger in size and more abundant toward the margins of those grains. In places, apatite is concentrated in interstitial areas with oxides as late crystallized products. The volume of apatite increases sympathetically with oxide content, and the melanocratic diorite grades into nelsonite.

Geochemical analyses of apatite (Table 7) show slightly elevated iron contents due to small inclusions of oxide minerals within the grains. The bulk of the rare-earth elements are contained within apatite, as demonstrated by the flat, 10x-enriched slope of apatite rare-earth element abundance normalized against whole-rock rare-earth element concentrations (Fig. 9). The negative europium anomaly relative to the whole-rock composition probably reflects prior plagioclase fractionation, possibly at depth in the source region for magma generation.

Mesocratic diorite

Mesodiorite is distinguished from the meladiorite by its lighter greenish-gray color, coarser grain size, local porphyritic texture (Fig. 10), higher proportion of interstitial quartz, albite, and biotite, and lower proportions of apatite, Fe-Ti oxides, pyroxene, and hornblende (Table 1). Locally it contains patches of chlorite-rich pegmatite (grain size as large as 2 inches [5 centimeters] in diameter), and segregations or more likely inclusions up to 6.6 feet (2 meters) across of anorthosite. Late-stage deuteric alteration in the coarser-grained varieties is pronounced, with heavily sericitized plagioclase and abundant late

Table 2. Geochemical analyses of samples of the Philbrook pluton.

Sample	Rock type	SiO_2	TiO_2	Al_2O_3	Fe_2O_3*	MnO	MgO	CaO	Na_2O	K_2O	P_2O_5	LOI	Sum
PB-1-OC	Mld	42.1	4.32	12.9	15.6	0.256	6.24	11.4	2.60	0.61	2.1	-	99.6
PB-3-1-74	Ox-mld	32.3	5.60	2.94	39.1	0.532	6.79	9.28	0.401	0.120	1.34	-	98.4
PB-3-5-179	Ox	20.8	12.9	2.25	49.4	0.673	3.92	7.20	0.192	0.1	0.13	-	97.54
PB-88-1-23**	Mld	39.07	6.61	10.57	20.78	0.24	6.75	9.58	1.72	0.65	0.39	0.82	97.18
PB01	Mld	40.11	4.91	12.33	18.53	0.24	6.40	11.89	2.28	0.25	2.57	0.94	100.43
PB02	Mld	42.55	5.81	11.29	20.41	0.27	6.26	10.20	2.17	0.96	0.57	0.16	100.66
PB06	Mld	40.39	4.46	11.78	19.39	0.26	6.58	11.38	2.55	0.54	2.36	0.60	100.29
PB08	Mld	35.45	4.94	12.94	18.80	0.27	5.49	11.78	3.28	0.19	2.72	5.00	100.85
PB09	Mld	40.39	4.50	12.62	18.58	0.25	6.11	11.57	2.79	0.56	2.42	0.27	100.05
PB10	Mld	46.67	2.60	18.72	11.10	0.16	2.93	10.60	4.35	0.46	1.37	0.75	99.72
PB11	Mld	41.88	4.37	12.75	17.09	0.24	6.00	11.93	2.60	0.65	2.25	0.45	100.19
PB12	Mld/Msd	40.89	4.44	11.92	19.04	0.25	6.50	11.71	2.44	0.58	2.38	0.23	100.37
PB13	Mld/Msd	40.32	4.44	12.24	19.29	0.25	5.96	11.01	2.70	0.60	2.47	0.59	99.86
PB14	Mld/Msd	40.19	4.84	11.90	20.15	0.27	5.82	10.65	2.58	0.94	2.57	0.52	100.44
PB05	Msd	47.10	2.75	17.81	12.30	0.17	4.01	8.90	3.57	1.21	0.29	1.97	100.09
PB15	Msd	44.21	3.57	13.45	15.15	0.23	4.52	11.12	3.48	0.67	2.01	1.94	100.36
PB16	Msd	48.23	0.58	21.11	8.18	0.11	3.27	9.98	4.53	0.32	0.14	3.97	100.41
PB17	Msd	49.95	1.20	23.94	5.46	0.08	1.65	10.26	4.93	0.48	0.23	1.10	99.28
PB18	Msd	48.92	0.83	22.94	7.47	0.09	2.97	9.49	4.60	0.45	0.21	1.57	99.52
PB20	Msd	46.97	2.15	19.64	10.90	0.14	3.68	9.95	3.27	0.73	0.26	1.62	99.33
PB-1-57	Ox	-	-	-	-	-	-	-	-	-	-	-	-
PB-3-72	Ox	-	-	-	-	-	-	-	-	-	-	-	-
PB-3-132	Ox	-	-	-	-	-	-	-	-	-	-	-	-
PB-5-208	Ox	-	-	-	-	-	-	-	-	-	-	-	-
PB-8-55	Hbt	-	-	-	-	-	-	-	-	-	-	-	-
PBI-2-88	Msd	-	-	-	-	-	-	-	-	-	-	-	-
PB-OC-PG	Msd	-	-	-	-	-	-	-	-	-	-	-	-

Values in weight percent oxides

* For sample PB-1-OC, Fe_2O_3 = 2.8 and FeO= 14.2. FeO was not determined for any other samples.

Sample	V	Cr	Co	Ni	Cu	Zn	Rb	Sr	Y	Zr	Ba	Pb	Th	U	Hf
PB-1-OC	390	3.9	61	6	53	150	7	400	45	123	520	-	-	-	-
PB-3-1-74	673	18	65	39	97	215	1.0	45.6	36.9	122	34.9	-	-	-	-
PB-3-5-179	529	5	46	17	11	535	2.0	25.4	18.1	114	69.7	-	-	-	-
PB-88-1-23	261	29	68.6	54.4	86.8	166	11.9	235	20	0.5	444	-	-	-	-
PB01	434.40	bd	59.25	3.00	84.04	155.80	2.40	446.50	47.95	81.85	354.25	2.45	8.60	1.60	2.50
PB02	669.94	0.23	59.23	31.00	66.66	184.23	23.17	298.23	36.80	180.93	857.50	4.07	9.23	1.33	2.20
PB06	379.66	bd	63.15	3.50	70.58	174.30	9.10	383.35	46.80	86.20	578.45	4.20	11.25	1.65	3.75
PB08	391.44	bd	49.65	2.60	16.58	149.60	2.30	296.30	48.75	103.45	205.15	1.50	8.75	1.25	2.75
PB09	383.69	bd	51.35	2.75	39.73	152.80	8.90	364.50	46.90	83.00	614.80	3.75	9.25	1.65	2.70
PB10	222.98	bd	27.55	2.45	17.82	155.45	8.65	994.35	26.35	92.90	808.10	23.55	8.90	3.90	0.90
PB11	386.91	bd	54.45	4.75	58.46	148.50	12.10	397.75	46.35	95.40	656.25	2.30	9.10	1.50	2.00
PB12	415.36	bd	48.45	3.45	62.91	144.40	10.75	409.10	47.55	96.55	613.20	2.95	8.55	1.70	2.75
PB13	373.62	bd	50.10	3.50	42.06	162.70	12.70	382.30	53.60	110.25	636.60	2.80	9.20	1.70	0.25
PB14	365.29	bd	52.45	3.90	62.22	181.80	21.55	372.15	55.85	149.85	832.05	3.55	10.45	0.45	4.00
PB05	472.28	3.85	35.45	16.05	26.51	210.95	59.65	1038.35	18.70	87.55	903.75	7.05	8.25	4.90	2.20
PB15	309.58	bd	33.90	2.40	23.58	151.00	17.45	538.65	56.35	160.95	745.60	4.60	10.20	2.35	4.70
PB16	84.95	125.85	22.45	39.85	6.34	85.05	7.15	878.65	6.90	36.65	524.60	9.10	5.75	2.80	0.00
PB17	180.12	124.85	13.80	16.40	7.86	51.10	10.85	770.45	11.60	63.40	623.05	5.70	5.65	2.75	0.00
PB18	124.93	108.75	21.90	28.70	6.09	81.85	9.75	681.90	9.50	40.15	533.50	4.35	5.75	3.05	0.15
PB20	488.28	10.50	31.80	20.80	23.55	120.50	14.10	548.00	19.00	92.20	650.50	4.40	5.70	1.50	4.00
PB-1-57	-	-	-	-	-	-	-	-	15	-	-	-	<1	<1	
PB-3-72	-	-	-	-	-	-	-	-	32	-	-	-	<1	<1	
PB-3-132	-	-	-	-	-	-	-	-	84	-	-	-	1	<1	
PB-5-208	-	-	-	-	-	-	-	-	95	-	-	-	<1	<1	
PB-8-55	-	-	-	-	-	-	-	-	48	-	-	-	2	<1	
PBI-2-88	-	-	-	-	-	-	-	-	46	-	-	-	1	<1	
PB-OC-PG	-	-	-	-	-	-	-	-	9	-	-	-	<1	<1	

Values in parts per million

Table 2. Continued.

Sample	La	Ce	Pr	Nd	Sm	Eu	Gd	Tb	Dy	Ho	Er	Tm	Yb	Lu
PB-1-OC	-	-	-	-	-	-	-	-	-	-	-	-	-	-
PB-3-1-74	-	-	-	-	-	-	-	-	-	-	-	-	-	-
PB-3-5-179	99.0	233.0	-	136.0	33.9	7.9	-	4.3	-	-	-	-	5.7	0.7
PB-88-1-23**	22.5	45.6	-	-	-	-	-	-	-	-	-	-	-	-
PB01	42.20	114.30	-	77.60	11.55	-	-	-	-	-	-	-	3.00	-
PB02	30.27	78.83	-	46.87	4.47	-	-	-	-	-	-	-	3.43	-
PB06	38.60	104.70	-	69.00	13.95	-	-	-	-	-	-	-	2.40	-
PB08	46.75	109.00	-	71.90	13.05	-	-	-	-	-	-	-	3.15	-
PB09	43.65	108.30	-	73.35	10.80	-	-	-	-	-	-	-	4.35	-
PB10	37.30	59.50	-	37.15	5.15	-	-	-	-	-	-	-	3.15	-
PB11	40.60	100.35	-	64.30	9.65	-	-	-	-	-	-	-	2.40	-
PB12	48.45	113.90	-	70.80	10.85	-	-	-	-	-	-	-	2.95	-
PB13	49.40	118.15	-	75.80	11.50	-	-	-	-	-	-	-	3.75	-
PB14	55.95	137.50	-	81.60	13.85	-	-	-	-	-	-	-	7.15	-
PB05	17.40	33.55	-	23.00	3.90	-	-	-	-	-	-	-	1.30	-
PB15	53.80	142.25	-	84.55	13.85	-	-	-	-	-	-	-	4.50	-
PB16	10.00	20.55	-	9.45	bd	-	-	-	-	-	-	-	0.35	-
PB17	26.10	30.60	-	16.40	0.85	-	-	-	-	-	-	-	1.55	-
PB18	16.40	28.45	-	10.05	bd	-	-	-	-	-	-	-	1.60	-
PB20	23.60	44.90	-	24.50	bd	-	-	-	-	-	-	-	3.90	-
PB-1-57	17.8	45.6	6.8	30.4	6.0	1.69	6.0	0.7	3.6	0.74	1.6	0.3	1.1	0.18
PB-3-72	36.3	93.4	14.4	67.7	12.9	3.59	11.5	1.3	7.3	1.49	3.4	0.5	2.3	0.35
PB-3-132	92.7	248	36.5	173	33.4	8.34	30.7	3.5	17.8	3.72	8.2	1.0	5.3	0.77
PB-5-208	92.1	234	34.4	174	32.8	8.38	28.4	3.9	19.6	3.76	10.0	1.1	6.6	0.81
PB-8-55	49.3	114	17.7	75.6	14.4	4.02	14.7	1.7	8.9	1.97	5.6	0.8	4.9	0.75
PBI-2-88	48.1	115	15.7	81.2	13.9	3.75	14.0	1.8	8.5	1.61	4.4	0.6	2.7	0.40
PB-OC-PG	13.3	27.9	3.4	14.3	2.4	1.62	2.5	0.3	1.7	0.34	1.1	0.2	1.0	0.19

Values in parts per million

Methods: Samples PB-1-OC, PB-3-1-74, and PB-3-5-179—Direct Current Plasma Atomic Emission Spectrometer (DCP-AES).

PB01 through PB18—Major and trace elements were analyzed by wavelength dispersive x-ray fluorescence. Major elements from fused "glass beads" composed of the sample and lithium metaborate and lithium tetraborate. Trace element concentrations were determined from pressed powder pellets. Analyses by Macalester College.

REE/Trace only samples—Inductively coupled plasma mass spectrometry (ICP-MS), X-Ray Assay Laboratories

Rock type abbreviations: Mld—Melanocratic diorite; Ox-mld—Oxide-rich meladiorite; Ox—Oxide and oxide-apatite rock (nelsonite); Msd—Mesocratic diorite; Hbt—Hornblendite

**Reported in Jirsa and others (2006).

- = Not determined bd = Below detection limit

veins and abrupt, patchy, epidote-zeolite-carbonate alteration zones. The rock color is largely controlled by the extent to which feldspar is altered whereby sericitized plagioclase is white and fresh plagioclase (andesine verging on labradorite; Table 3, An_{45-53}) is gray; less-altered feldspar crystals are selectively saussuritized in the cores. Interstitial albite (An_{03-10}), similar to that in the melanocratic diorite, is fresh and lacks the fine Fe-oxide dust that characterizes the andesine crystals. The mafic component is dominantly subpoikilitic hornblende, as well as secondary actinolite and chlorite, all of which are at least partly, or more likely entirely, secondary after magmatic pyroxene. Apatite is typically coarser-grained but less abundant than in the melanocratic phase, and is similarly associated with Fe-Ti oxides as a late crystallization product.

The plagioclase in the anorthosite inclusions is generally more calcic (labradorite; Table 3) than that in the diorite, implying that it may be an inclusion of an earlier-crystallized phase brought up from depth. Patches of epidote alteration and fracture fillings correspond to sericitized zones, and alteration has variably obliterated the primary rock texture. In contrast to the slight negative Eu anomalies in the other phases of the intrusion, the anorthosite has a

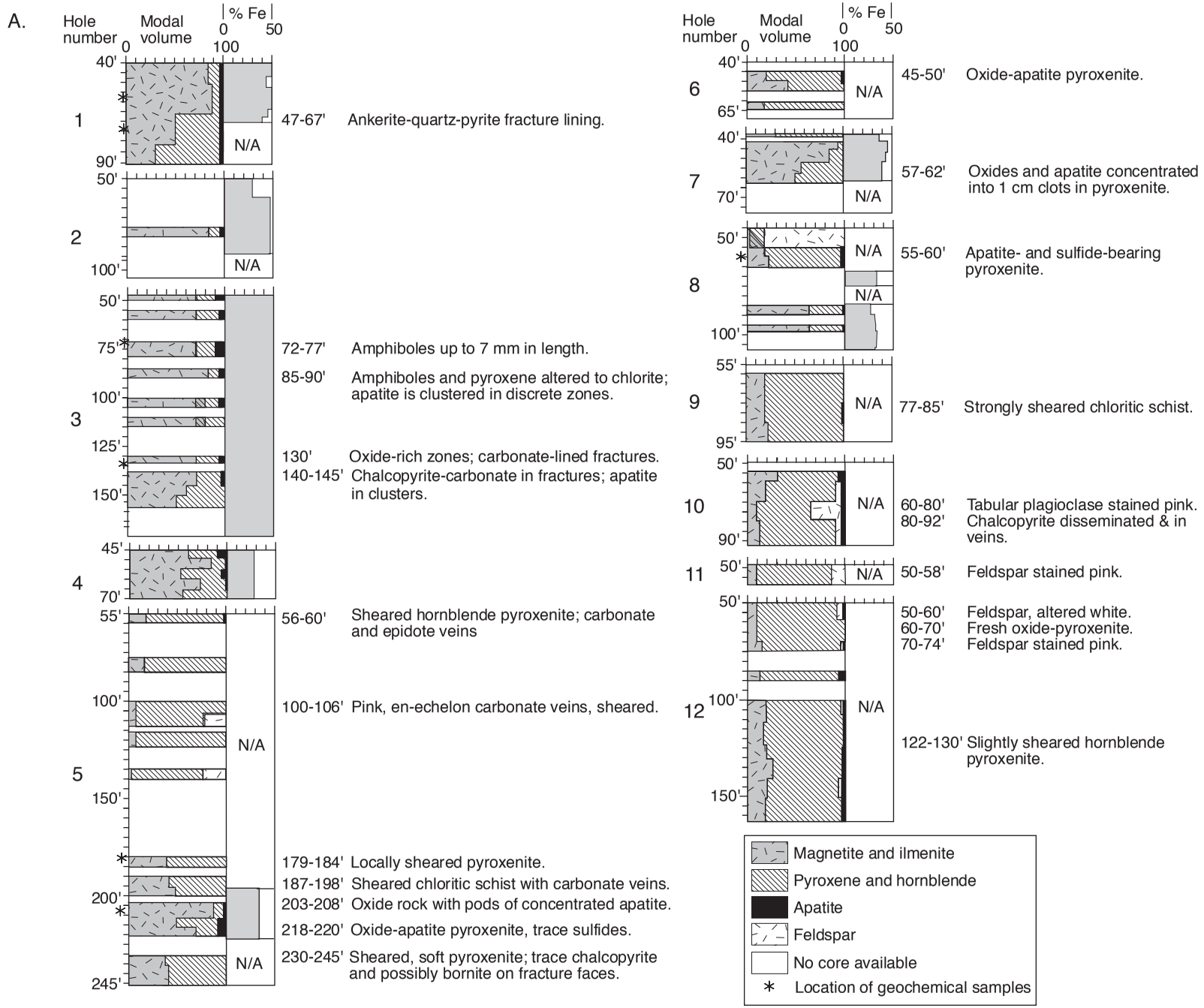
A.
Hole number
Modal volume
% Fe
0
100
0
50
1
40'
90'
N/A
47-67' Ankerite-quartz-pyrite fracture lining.
2
50'
100'
N/A
3
50'
75'
100'
125'
150'
72-77' Amphiboles up to 7 mm in length.
85-90' Amphiboles and pyroxene altered to chlorite; apatite is clustered in discrete zones.
130' Oxide-rich zones; carbonate-lined fractures.
140-145' Chalcopyrite-carbonate in fractures; apatite in clusters.
4
45'
70'
5
55'
100'
150'
200'
245'
N/A
56-60' Sheared hornblende pyroxenite; carbonate and epidote veins
100-106' Pink, en-echelon carbonate veins, sheared.
179-184' Locally sheared pyroxenite.
187-198' Sheared chloritic schist with carbonate veins.
203-208' Oxide rock with pods of concentrated apatite.
218-220' Oxide-apatite pyroxenite, trace sulfides.
230-245' Sheared, soft pyroxenite; trace chalcopyrite and possibly bornite on fracture faces.
6
40'
65'
45-50' Oxide-apatite pyroxenite.
7
40'
70'
57-62' Oxides and apatite concentrated into 1 cm clots in pyroxenite.
8
50'
100'
55-60' Apatite- and sulfide-bearing pyroxenite.
9
55'
95'
77-85' Strongly sheared chloritic schist.
10
50'
90'
60-80' Tabular plagioclase stained pink.
80-92' Chalcopyrite disseminated & in veins.
11
50'
50-58' Feldspar stained pink.
12
50'
100'
150'
50-60' Feldspar, altered white.
60-70' Fresh oxide-pyroxenite.
70-74' Feldspar stained pink.
122-130' Slightly sheared hornblende pyroxenite.
Magnetite and ilmenite
Pyroxene and hornblende
Apatite
Feldspar
No core available
Location of geochemical samples

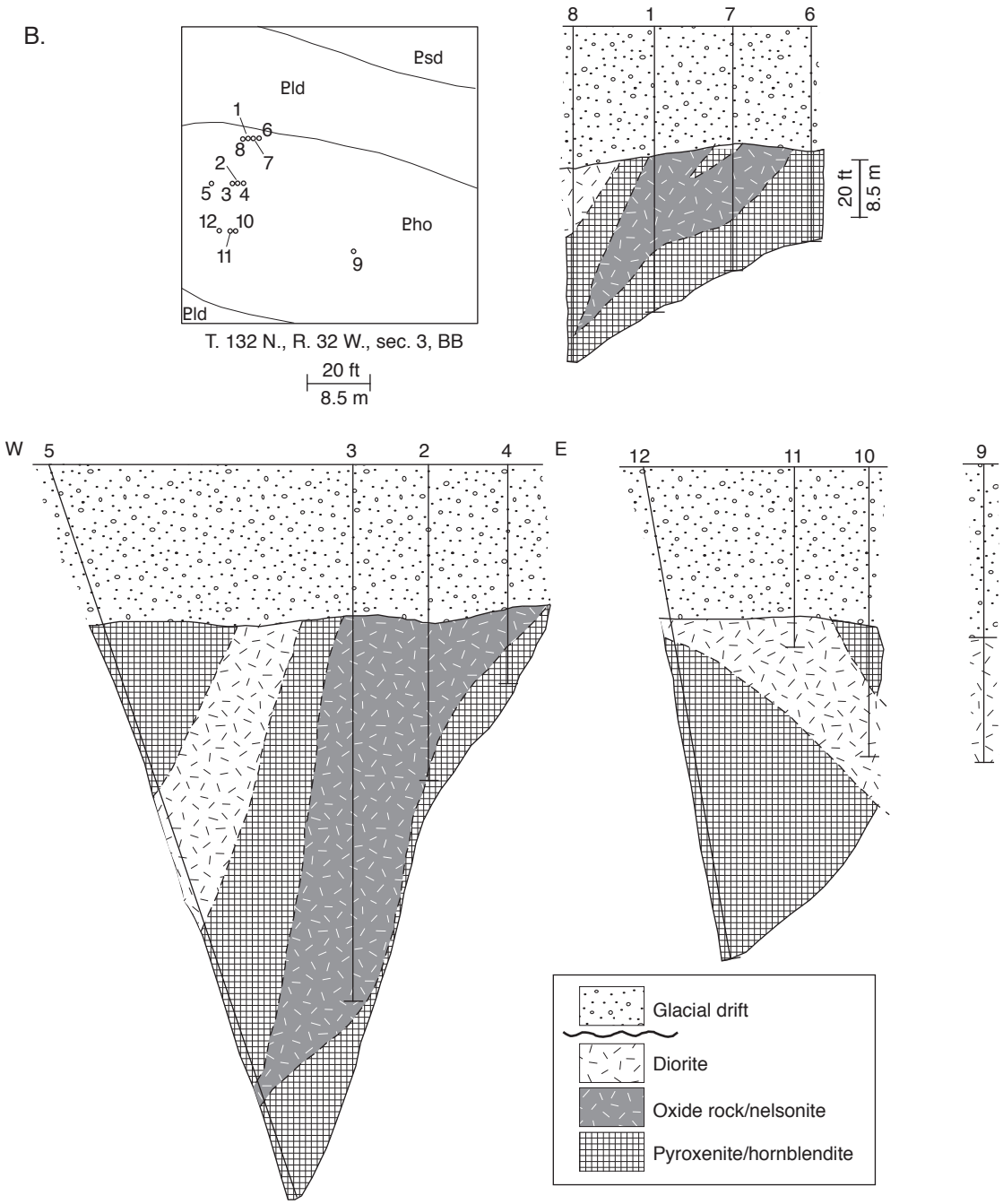

Figure 4. A. Graphic representation of drill cores drilled by Adams Exploration. The modal volume is based on visual examination of the drill cores by the author. For those parts of the core now missing due to skeletonization, the percentage of iron (taken from Adams Exploration drilling assay data) was used to infer oxide contents.

B. Drill array cross sections based on drill cores and drill logs (Fig. 4A). Locations of the drill holes are shown in the inset box; see Figure 2A for the locations of the holes relative to the intrusion. Cross sections face north.

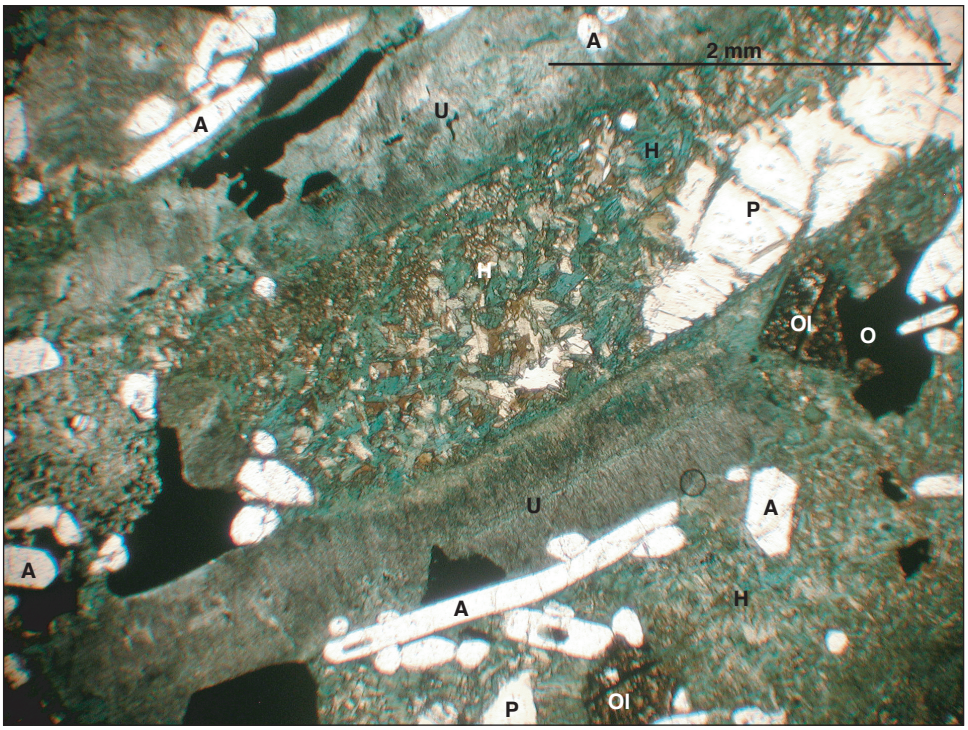

Figure 5. Photomicrograph of melanocratic ferrodiorite showing prismatic apatite (A), uralitized pyroxene (U), opaque Fe-Ti oxides (O), possible olivine pseudomorphs (Ol), and plagioclase (P) with typical partial replacement by green ferroan pargasite hornblende (H). Photographed in plane polarized light; from outcrop sample PB-1.

Figure 6. Locally derived corestone boulder of Philbrook-intrusion diorite showing modal layering.

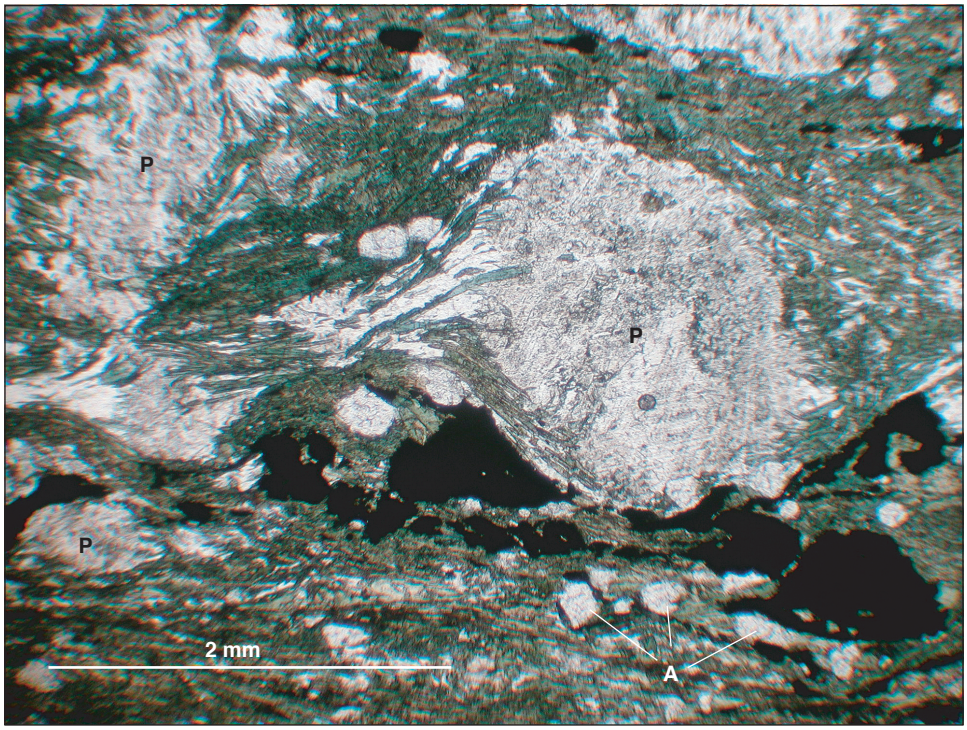

Figure 7. Photomicrograph of protomylonitic diorite from a narrow, north–northwest-trending brittle shear zone near the mouth of Fish Trap Creek. P—plagioclase feldspar; A—apatite. Prismatic green crystals are amphiboles. Photographed in plane-polarized light.

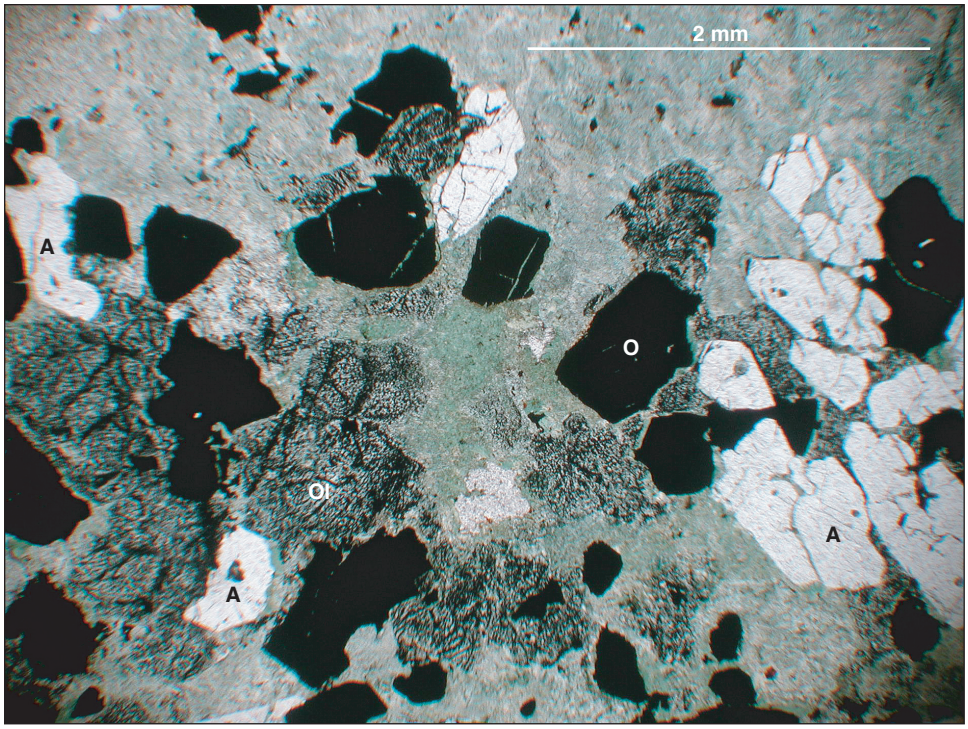

Figure 8. Photomicrograph of rock classified as hornblendite showing possible olivine pseudomorphs (Ol), blocky magnetite with exsolved ilmenite lamellae (not visible; O), and large, subpoikilitic apatite grains (A). Gray background is composed entirely of fine-grained, felty-fibrous amphibole. Photographed in plane-polarized light.

Table 3. Microprobe analyses of feldspar.

	Weight percent oxides							Number of ions based on 8(O) in formula											
Sample	SiO_2	Al_2O_3	FeO	CaO	Na_2O	K_2O	Total	Si	Al	Ca	Na	K	Fe	Cation sum	Or	Ab	An	Si+Al	Ca+Na
P11-10	54.81	28.47	0.16	10.27	5.84	0.16	99.71	2.48	1.52	0.50	0.51	0.01	0.01	2.72	1	50	49	4.00	1.01
P13-10	56.23	27.55	0.1	9.28	6.34	0.13	99.63	2.54	1.46	0.45	0.55	0.01	0.00	2.71	1	55	44	4.00	1.00
P14-1	55.25	27.71	0.15	9.38	6.31	0.14	98.94	2.51	1.49	0.46	0.56	0.01	0.01	2.73	1	54	45	4.00	1.01
P1-OG	55.41	27.74	0.24	9.29	6.35	0.21	99.24	2.51	1.48	0.45	0.56	0.01	0.01	2.73	1	55	44	4.00	1.01
P2-OG	55.96	27.57	0	9.31	6.45	0.13	99.42	2.53	1.47	0.45	0.57	0.01	0.00	2.72	1	55	44	4.00	1.02
P2'-OG	55.06	27.56	0.13	9.84	6.3	0.14	99.03	2.51	1.48	0.48	0.56	0.01	0.00	2.74	1	53	46	3.99	1.04
P5-PG	57.13	27.69	0	9.34	6.54	0.13	100.83	2.54	1.45	0.45	0.56	0.01	0.00	2.68	1	55	44	4.00	1.01
P6-OG	55.82	27.58	0	9.38	6.5	0.13	99.41	2.53	1.47	0.45	0.57	0.01	0.00	2.72	1	55	44	4.00	1.02
P7-OG	55.95	27.06	0	8.66	6.99	0.11	98.77	2.54	1.45	0.42	0.62	0.01	0.00	2.73	1	59	40	4.00	1.04
P8-OG	54.71	27.54	0.23	9.66	6.2	0.15	98.49	2.50	1.49	0.47	0.55	0.01	0.01	2.75	1	53	46	3.99	1.02
P9-OG	55.21	27.68	0.05	9.46	6.34	0.14	98.88	2.51	1.49	0.46	0.56	0.01	0.00	2.73	1	54	45	4.00	1.02
PTH1-OG	62.71	21.93	0	3.98	9.17	0.11	97.9	2.83	1.17	0.19	0.80	0.01	0.00	2.71	1	80	19	3.99	0.99
PTH2-OG	65.95	20.46	0	1.42	11.37	0.11	99.31	2.92	1.07	0.07	0.98	0.01	0.00	2.66	1	93	6	3.99	1.04
PTH3-OG	67.38	19.66	0	0.63	11.87	0.18	99.72	2.96	1.02	0.03	1.01	0.01	0.00	2.64	1	96	3	3.98	1.04
P16-PA	50.73	27.54	0	10.06	5.33	0.15	93.81	3.24	1.56	0.52	0.50	0.01	0.00	2.89	1	49	51	4.81	1.02
P17-PA	52.26	28.42	0.08	10.6	5.3	0.16	96.82	2.37	1.56	0.53	0.48	0.01	0.00	2.80	1	47	52	3.93	1.01
P18-PA	52.7	26.05	0.07	9.33	5.74	0.15	94.04	2.50	1.47	0.48	0.53	0.01	0.00	2.88	1	52	47	3.97	1.01
P19-PA	50.24	28.06	0.14	10.56	5.01	0.16	94.17	2.53	1.59	0.54	0.47	0.01	0.01	2.89	1	46	53	4.12	1.01

P11-10; P13-10—Mesocratic diorite in outcrop, T. 133 N., R. 32 W., sec. 34, ADAA
P14-1—Melanocratic diorite in outcrop, T. 133 N., R. 32 W., sec. 34, BBAD
P1-OG to PTH3-OG—Melanocratic diorite in outcrop, T. 133 N., R. 32 W., sec. 34, DCAB
P16-PA to P19-PA—Anorthosite, T. 133 N., R. 32 W., sec. 34, CADB

Table 4. Microprobe analyses of pyroxene.

	Weight percent oxides										Number of ions based on 6(O) in formula														
Sample	SiO_2	TiO_2	Al_2O_3	FeO	MnO	MgO	CaO	Na_2O	K_2O	Total	Si	Ti	Al	Fe	Mn	Mg	Ca	Na	K	Cation sum	En	Fs	Wo	Si+Al	En'
PX2-OG	51.35	0.65	2.85	11.66	0.3	12.52	19.73	0.49	0.12	99.67	1.94	0.02	0.13	0.37	0.01	0.70	0.80	0.04	0.01	2.27	37.46	20.09	42.45	2.06	65.094
PX3-OG	50.08	0.93	2.41	11.57	0.27	11.96	20.5	0.51	0.11	98.34	1.93	0.03	0.11	0.37	0.01	0.69	0.84	0.04	0.01	2.31	35.87	19.93	44.20	2.03	64.28
PX3A-OG	50.12	0.47	3.13	13.65	0.23	12.24	17.51	0.47	0.15	97.97	1.93	0.01	0.14	0.44	0.01	0.70	0.72	0.04	0.01	2.32	37.52	23.88	38.59	2.07	61.106
PX5-74	51.18	0.04	0.14	15.35	0.39	9.3	23.03	0.18	0.1	99.71	1.99	0.00	0.01	0.50	0.01	0.54	0.96	0.01	0.00	2.33	26.81	25.47	47.73	1.99	51.28
PX6-74	50.82	0	0.03	14.1	0.36	9.84	23.35	0.18	0.1	98.78	1.98	0.00	0.00	0.46	0.01	0.57	0.98	0.01	0.00	2.35	28.32	23.36	48.32	1.99	54.797
PX7-74	51.22	0.04	0.04	14.39	0.47	9.17	23.84	0.18	0.09	99.44	1.99	0.00	0.00	0.47	0.02	0.53	0.99	0.01	0.00	2.33	26.46	24.07	49.46	1.99	52.363
PX8-74	50.25	0	0.05	12.21	0.42	10.67	23.94	0.17	0.1	97.81	1.97	0.00	0.00	0.40	0.01	0.62	1.01	0.01	0.01	2.36	30.51	20.27	49.22	1.97	60.077

En' = (Mg/Mg+Fe+Mn)*100

PX2-OG, 3-OG, and 3A-OG—Brownish augite heavily mantled and replaced by hornblende; from mesocratic diorite outcrop, T. 133 N., R. 32 W., sec. 34, BACCD
PX5-74 through PX8-74—Colorless, clean, weakly uralitized calcium-rich augite, from hornblende pyroxenite, drill core 1, 74-80' interval; T. 132 N., R. 32 W., sec. 3

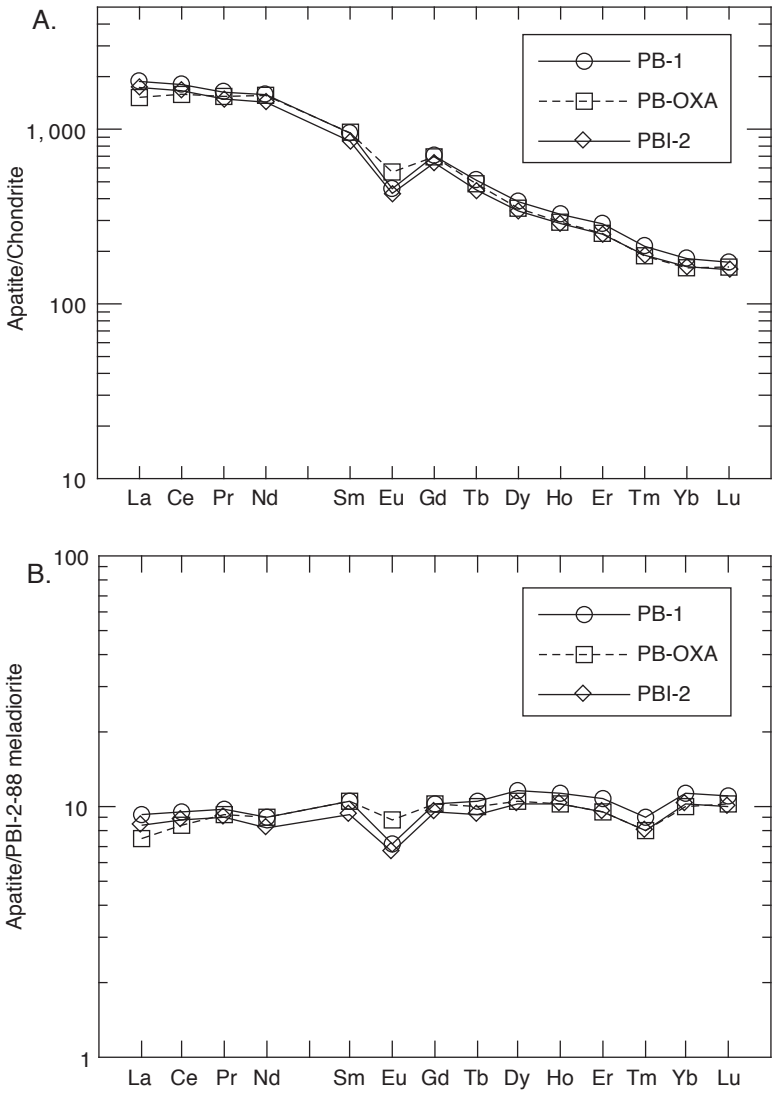

Figure 9. A. Rare-earth element contents of apatite normalized to chondrite values using the RockWare Igpet program (Sun and McDonough, 1989).

B. Rare-earth element contents of apatite normalized to whole rock sample PBI-2-88 (Table 2; melanocratic ferrodiorite). See Table 7 for analyses of apatite separates. Samples PB-1 and PBI-2 are from melanocratic diorite; sample PB-OXA is from oxide-apatite rock.

pronounced positive europium anomaly (as shown in Fig. 11), further evidence of xenoliths brought up from a sub-crustal anorthositic magma chamber.

The blue-green prismatic ferropargasitic amphibole (Table 5A, samples HB-1-OG through HB-4-OG; type 2 under Meladiorite), and fibrous actinolite (Table 5A, sample HB-5-OG; type 1 under Meladiorite) are the most common amphibole types in samples from outcrops of this rock type. Minor amounts of an army-green amphibole forms subpoikilitic grains and appears to be magmatic, but is more likely a deuteric alteration product after pyroxene because it is chemically closer to actinolite (Table 5A, samples HB-5-10 and HB-6-10; Fig. 12).

Pyroxenite and hornblendite

Dark green, medium-grained magnetite-hornblende pyroxenite and magnetite hornblendite comprise approximately 80 percent of the available drill core, but are not exposed in outcrop. Oxide contents vary from 10 percent to more than 80 percent, the latter grading into oxide rock, and apatite accounts for 2 to 20 percent of the rock volume (Table 1); oxide-apatite rock also locally forms discrete clots. Pyroxenite is dark green, massive, and equigranular, whereas hornblendite is typically more coarse-grained, lighter green, and dominated by felty intergrowths of prismatic actinolite and hornblende of secondary origin. Approximately 40 percent of the hornblendite in drill core has been sheared and retrograded to a soft, splintery, lineated chloritic actinolite schist, presumably along northwest-trending shear zones similar to those noted in outcrops. The volume of primary magmatic hornblende (Fig. 13) is greatest in the hornblende pyroxenite, and secondary

Table 5A. Microprobe analyses of amphiboles from diorites.

MELANOCRATIC DIORITE

	Weight percent oxides										Number of ions based on 23(0) in formula									
Sample	SiO_2	TiO_2	Al_2O_3	FeO	MnO	MgO	CaO	K_2O	Na_2O	Total	Si	Ti	Al	Fe	Mn	Mg	Ca	K	Na	Cation sum
HB-35-1	41.74	0.36	14.27	20.94	0.23	7.04	11.61	0.54	1.7	98.43	6.23	0.045	2.51	2.609	0.027	1.569	1.856	0.099	0.493	15.438
HB-36-1	39.98	0.25	16.14	21.31	0.23	5.82	11.45	0.65	1.86	97.69	6.051	0.027	2.885	2.703	0.027	1.31	1.856	0.127	0.546	15.532

Sample	Al IV	AL VI	Fe 3	Fe 2	(Ca+ Na)B	NaB	(Na+K)A	Mg/(Mg+ Fe2)	P1	P2	P3	Name
HB-35-1	1.77	0.74	0.656	1.954	2	0.144	0.448	0.445	21.006	28.713	1.441	Ferro-tschermakite
HB-36-1	1.949	0.936	0.568	2.134	2	0.144	0.529	0.38	22.738	32.283	1.531	Ferroan pargasite

HB-35-1—Blue-green inclusion-laden hornblende of possible magmatic origin in melanocratic diorite, T. 133 N., R. 32 W., sec. 34, DABB
HB-36-1—Blue-green hornblende of deuteric origin, same location as above

MESOCRATIC DIORITE

	Weight percent oxides										Number of ions based on 23(0) in formula									
Sample	SiO_2	TiO_2	Al_2O_3	FeO	MnO	MgO	CaO	K_2O	Na_2O	Total	Si	Ti	Al	Fe	Mn	Mg	Ca	K	Na	Cation sum
HB-1-OG	39.36	0.15	14.49	23.22	0.2	5.31	11.6	0.76	1.64	96.73	6.085	0.019	2.639	3	0.028	1.227	1.924	0.149	0.492	15.563
HB-2-OG	40.25	0.15	17.56	22.36	0.22	4.71	11.57	0.85	1.64	99.31	6.02	0.018	3.092	2.795	0.027	1.051	1.851	0.162	0.476	15.492
HB-3A-OG	39.79	0.24	15.63	22.15	0.24	5.64	11.52	0.69	1.7	97.6	6.045	0.027	2.803	2.812	0.027	1.278	1.872	0.137	0.502	15.503
HB-4-OG	39.02	0.35	17.93	21.36	0.21	4.91	11.53	0.78	1.69	97.78	5.915	0.036	3.208	2.707	0.027	1.112	1.878	0.155	0.501	15.539
HB-5-OG	56.77	0.28	2.39	14.12	0.21	10.78	10.67	0.14	0.45	95.81	8.249	0.035	0.411	1.72	0.027	2.331	1.658	0.027	0.131	14.589
HB-5-10	50.21	0.48	3.44	16.47	0.18	12.45	12.28	0.19	0.65	96.35	7.492	0.054	0.601	2.052	0.027	2.769	1.962	0.036	0.188	15.181
HB-6-10	50.08	0.1	3.4	16.4	0.14	12.71	12.22	0.2	0.63	95.88	7.494	0.009	0.602	2.051	0.018	2.834	1.961	0.036	0.18	15.185

Sample	Al IV	AL VI	Fe 3	Fe 2	(Ca+ Na)B	NaB	(Na+K)A	Mg/(Mg+ Fe2)	P1	P2	P3	Name
HB-1-OG	1.915	0.724	0.67	2.331	2	0.076	0.565	0.345	20.392	30.243	1.413	Ferroan pargasite
HB-2-OG	1.98	1.112	0.484	2.311	2	0.149	0.489	0.313	20.451	33.927	1.614	Alumino-ferro tschermakite
HB-3A-OG	1.955	0.848	0.686	2.127	2	0.128	0.511	0.375	21.153	31.679	1.561	Ferroan pargasite
HB-4-OG	2.085	1.123	0.468	2.239	2	0.122	0.534	0.332	21.066	35.168	1.627	Alumino-ferroan pargasite
HB-5-OG	0	0.411	0	1.72	1.789	0.131	0.027	0.575	7.314	4.741	0.446	Actinolite
HB-5-10	0.508	0.093	0.168	1.884	2	0.038	0.186	0.595	8.75	7.421	0.315	Actinolitic hornblende
HB-6-10	0.506	0.096	0.238	1.803	2	0.039	0.177	0.61	8.415	7.45	0.343	Actinolitic hornblende

HB-1-OG to HB-4-OG—Prismatic rims on pyroxene that penetrate adjacent feldspar crystals, mesocratic diorite outcrop, T. 133 N., R. 32 W., sec. 34, BACCD
HB-5-OG—Fibrous pale green amphibole after pyroxene, same sample as HB-1-OG to HB-4-OG
HB-5-10 and HB-6-10—Dark army-green amphibole of apparent deuteric origin, mesocratic diorite outcrop, T. 133 N., R. 32 W., sec. 34, BADAC

Table 5B. Microprobe analyses of amphiboles from pyroxenite and hornblendite. Drill-hole locations are shown on Figure 4B.

SECONDARY AMPHIBOLES

	Weight percent oxides										Number of ions based on 23(0) in formula									
Sample	SiO_2	TiO_2	Al_2O_3	FeO	MnO	MgO	CaO	K_2O	Na_2O	Total	Si	Ti	Al	Fe	Mn	Mg	Ca	K	Na	Cation sum
ACT-1-74	50.95	0.06	1.82	20.25	0.32	10.61	11.97	0.2	0.38	96.56	7.682	0.009	0.326	2.555	0.045	2.383	1.93	0.036	0.109	15.075
ACT-2-74	51.25	0	1.16	20.08	0.44	10.83	11.78	0.15	0.34	96.03	7.753	0	0.209	2.535	0.055	2.444	1.909	0.027	0.1	15.032

Sample	Al IV	AL VI	Fe 3	Fe 2	(Ca+Na)B	NaB	(Na+K)A	Mg/(Mg+Fe2)	P1	P2	P3	Name
ACT-1-74	0.318	0.008	0.288	2.267	2	0.07	0.075	0.512	5.314	4.07	0.305	Actinolite
ACT-2-74	0.209	0	0.348	2.187	2	0.091	0.036	0.528	4.988	2.63	0.348	Actinolite

MAGMATIC AMPHIBOLES

	Weight percent oxides										Number of ions based on 23(0) in formula									
Sample	SiO_2	TiO_2	Al_2O_3	FeO	MnO	MgO	CaO	K_2O	Na_2O	Total	Si	Ti	Al	Fe	Mn	Mg	Ca	K	Na	Cation sum
HB-19-20	37.88	1.71	13.54	25.07	0.35	4.24	11.46	1.05	1.93	97.23	5.955	0.198	2.514	3.299	0.047	0.992	1.928	0.208	0.586	15.727
HB-20-50	38.22	1.44	13.71	24.92	0.26	4.43	11.49	1.03	2.3	97.8	5.973	0.169	2.526	3.258	0.038	1.033	1.926	0.207	0.695	15.825
HB-21-50	47.45	0.22	4	21.44	0.32	9.82	11.31	0.27	0.93	95.76	7.243	0.028	0.715	2.732	0.046	2.237	1.852	0.055	0.275	15.183
HB-22-50	43.39	0.46	7.9	23.74	0.39	7.17	11.57	0.64	1.42	96.68	6.722	0.056	1.443	3.073	0.047	1.658	1.918	0.13	0.428	15.475
HB-23-50	47.57	0.09	3.32	21.67	0.38	9.32	11.86	0.33	0.69	95.23	7.375	0.009	0.605	2.812	0.047	2.151	1.965	0.065	0.205	15.234
HB-24-50	48.74	0.07	1.78	20.69	0.27	10.22	12.23	0.18	0.37	94.55	7.567	0.009	0.327	2.687	0.037	2.369	2.034	0.037	0.112	15.179
HB-25-50	50.03	0	0.42	21.42	0.27	10.02	12.24	0.12	0.16	94.68	7.776	0	0.075	2.782	0.037	2.324	2.035	0.028	0.047	15.104
HB-30-50	37.52	2.38	13.16	23.03	0.24	5.37	11.38	1.16	2.52	96.76	5.928	0.285	2.451	3.049	0.028	1.264	1.929	0.237	0.769	15.94
HB-31-50	46.98	0.11	2.54	21.49	0.35	9.26	11.8	0.23	0.53	93.29	7.44	0.01	0.475	2.844	0.048	2.188	1.998	0.048	0.162	15.213
HB-13'-74	40.58	2.49	12.38	22.2	0.02	6.05	11.47	1.43	2.45	99.3	6.213	0.285	2.236	2.844	0.037	1.381	1.886	0.276	0.727	15.885
HB-14-74	37.34	1.99	12.69	22.85	0.23	5.83	11.38	1.23	2.21	95.75	5.935	0.239	2.379	3.038	0.029	1.386	1.94	0.248	0.678	15.872
HB-16-74	46.82	0.11	1.63	21.38	0.4	9.92	11.61	0.23	0.43	92.53	7.437	0.01	0.305	2.845	0.057	2.349	1.976	0.048	0.134	15.161

Sample	Al IV	AL VI	Fe 3	Fe 2	(Ca+Na)B	NaB	(Na+K)A	Mg/(Mg+Fe2)	P1	P2	P3	Name
HB-19-20	2.045	0.469	0.52	2.778	2	0.072	0.722	0.263	23.298	29.689	1.187	Hastingsite
HB-20-50	2.027	0.499	0.444	2.814	2	0.074	0.828	0.268	26.531	29.722	1.112	Ferro-pargasite
HB-21-50	0.715	0	0.708	2.024	2	0.148	0.182	0.525	12.917	8.983	0.736	Magnesio-hornblende
HB-22-50	1.278	0.165	0.612	2.461	2	0.082	0.476	0.403	18.251	17.675	0.833	Ferro-hornblende
HB-23-50	0.605	0	0.426	2.386	2	0.035	0.235	0.474	9.452	7.585	0.435	Ferro actinolitic hornblende
HB-24-50	0.327	0	0.31	2.377	2.034	0	0.149	0.499	5.229	4.139	0.319	Ferro-actinolite
HB-25-50	0.075	0	0.24	12.542	2.035	0	0.075	0.478	2.245	0.95	0.24	Ferro-actinolite
HB-30-50	2.072	0.379	0.25	2.799	2	0.071	0.935	0.311	28.513	29.248	0.914	Titanian-ferroan pargasite
HB-31-50	0.475	0	0.41	2.434	2	0.002	0.208	0.473	7.484	6.012	0.42	Ferro actinolitic hornblende
HB-13'-74	1.787	0.449	0	2.844	2	0.114	0.889	0.327	27.822	26.474	0.734	Potassian-titanian-ferroan pargasite
HB-14-74	2.065	0.314	0.456	2.582	2	0.06	0.866	0.349	25.918	28.619	1.009	Magnesian hastingsite
HB-16-74	0.305	0	0.662	2.83	2	0.024	0.158	0.518	6.352	3.947	0.672	Actinolitic hornblende

ACT-1-74—Colorless to pale green actinolite in fibrous mats, in pyroxenite from drill hole 1, 74-80' depth
ACT-2-74—Actinolite after pyroxene, same sample as ACT-1-74
HB-19-20 and HB-20-50—Red-brown core of hornblende in hornblendite, drill hole 6, 50-53' depth
HB-21-50—Light green rim on above
HB-22-50—Dark green rim on above
HB-23-50—Light green rim on above
HB-24-50—Dark green rim on above
HB-25-50—Light green rim on above
HB-30-50—Red-brown core of cumulus hornblende crystal, drill hole 6, 50-53' depth
HB-31-50—Colorless rim on above
HB-13'-74 and HB-14-74—Red-brown hornblende core, in pyroxenite from drill hole 1, 74-80' depth
HB-16-74—Colorless rim on above

Table 6. Microprobe analyses of sphene, calcite, and biotite. Drill-hole locations are shown on Figure 4B.

	Weight percent oxides										Number of ions based on x[1](O) in formula									
Sample	SiO_2	TiO_2	Al_2O_3	FeO	MnO	MgO	CaO	Na_2O	K_2O	Total	Cation sum	Si	Ti	Al	Fe	Mn	Mg	Ca	Na	K
SP74-11	30.32	36.97	0.24	1.49	0.04	0.12	29.16	0.09	0.1	98.53	8.04	4.06	3.72	0.04	0.17	0.00	0.02	4.18	0.02	0.02
SP74-14	28.33	37.2	0.31	1.41	0.02	0.13	28.81	0.1	0.09	96.4	8.26	3.89	3.84	0.05	0.16	0.00	0.03	4.24	0.03	0.02
SP2-136	32.58	38.46	0.57	1.06	0	0	28.96	0	0	101.63	7.71	4.18	3.71	0.09	0.11	0.00	0.00	3.98	0.00	0.00
CB50-25	0	0	0	0.95	0.36	0.23	54.99	0.11	0.08	56.72	5.96	0.00	0.00	0.00	0.08	0.03	0.03	5.84	0.02	0.01
BI-OG6	34.53	1.79	17.2	23.17	0.12	8.323	0.3	0.17	9.69	95.293	10.25	5.89	0.23	3.46	3.30	0.02	2.12	0.05	0.06	2.11
BI1-27	35.01	2.33	17.04	22.04	0.11	8.36	0.18	0.12	10.14	95.33	10.20	5.94	0.30	3.41	3.13	0.02	2.11	0.03	0.04	2.20

[1]x = 20 for sphene, 6 for calcite, and 24 for biotite

SP74-11 and SP74-14—Interstitial sphene from magnetite pyroxenite, drill hole 1, 74' depth
SP2-136—Interstitial sphene in oxide rock, drill hole 3, 136' depth
CB50-25—Interstitial calcite in magnetite hornblendite, drill hole 6
BI-OG6—Biotite, from melanocratic diorite outcrop, T. 133 N., R. 32 W., sec. 34, BACD
BI1-27—Biotite, from melanocratic diorite outcrop, T. 133 N., R. 32 W., sec. 34, CABB

Table 7. Geochemical analyses of apatite concentrates. Drill-hole locations are shown on Figure 4B.

Sample	SiO_2	TiO_2	Al_2O_3	MgO	Fe_2O_3	MnO	CaO	Na_2O	K_2O	P_2O_5	Sum
PB-1	7.18	0.08	3.02	0.15	0.59	0.04	49.21	0.80	0.07	39.39	100.52
PB-OXA	1.20	0.08	0.24	0.14	0.56	0.05	53.79	0.05	0.01	44.52	100.63
PBI-2	4.32	0.08	1.32	0.20	0.59	0.03	51.16	0.54	0.05	41.68	99.97

Weight percent oxides

	Rb	Ba	Sr	Be	V	Cr	Co	Ni	Cu	Zn	Ga	Y	Zr	Cs	Th	Hf	U	Pb	Y
PB-1	0.83	96.80	721.37	0.23	14.51	3.22	1.48	10.94	17.64	5.12	11.58	501.63	10.62	0.00	9.46	0.44	2.01	4.85	488.71
PB-OXA	0.30	30.67	586.04	0.01	18.45	3.15	4.00	10.43	41.25	29.41	9.00	445.40	9.78	0.00	2.88	0.36	0.74	7.10	430.88
PBI-2	1.05	56.99	533.59	0.12	22.94	3.13	1.71	9.06	22.83	7.28	9.34	448.79	16.30	0.00	8.86	0.42	1.90	4.13	438.28

Parts per million

	La	Ce	Pr	Nd	Sm	Eu	Gd	Tb	Dy	Ho	Er	Tm	Yb	Lu
PB-1	444.44	1102.72	154.78	736.68	145.13	26.48	144.54	19.10	97.63	18.40	47.57	5.44	30.88	4.40
PB-OXA	360.46	970.82	146.47	728.34	145.95	32.94	142.83	18.20	89.41	16.65	41.85	4.79	27.34	4.13
PBI-2	410.28	1015.93	141.47	666.11	130.45	24.89	131.85	16.80	86.32	16.32	41.45	4.84	27.76	3.99

Parts per million

PB-1—Prismatic apatite from melanocratic diorite outcrop, T. 133 N., R. 32 W., sec. 34, BCDA
PB-OXA—Prismatic apatite from oxide-apatite rock, drill hole 1, 57' depth
PBI-2—Prismatic apatite from melanocratic diorite in drill core PBI-88-2, 30' depth, T. 132 N., R. 32 W., sec. 3, BAAAA

Analyses by Rick Knurr, University of Minnesota Department of Geology

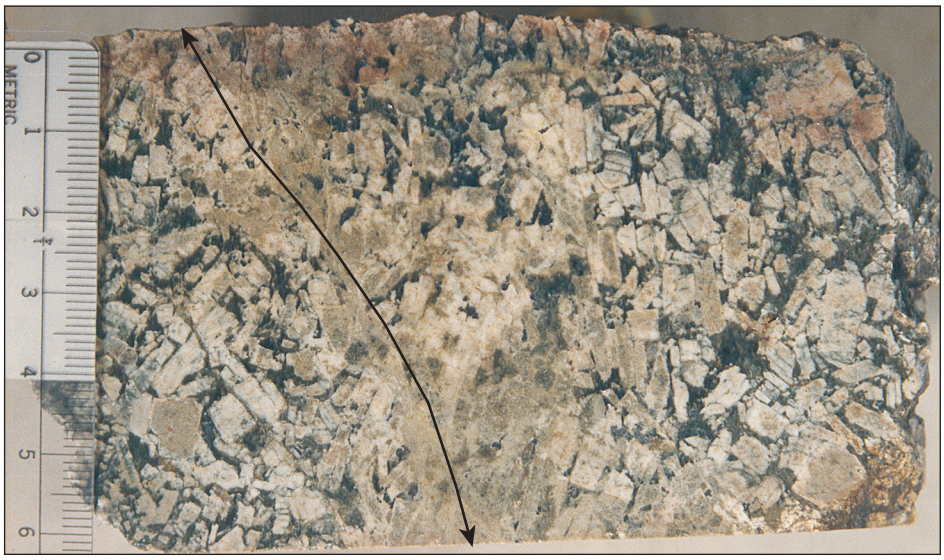

Figure 10. Photograph of porphyritic mesocratic diorite. Note the alteration zone that extends from the top to the bottom (arrow).

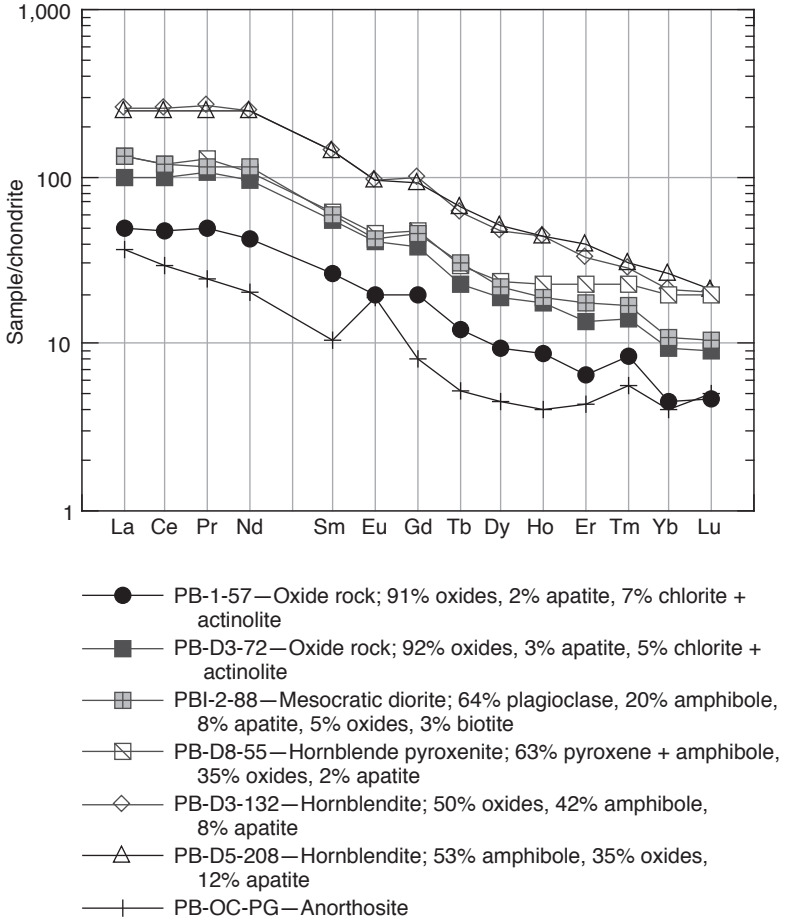

Figure 11. Chondrite-normalized rare-earth element patterns of samples from the Philbrook intrusion. The rare-earth element content and pattern closely follows, and is largely controlled, by that of apatite (Fig. 9). Chondrite standard of Taylor and McClennan (1985).

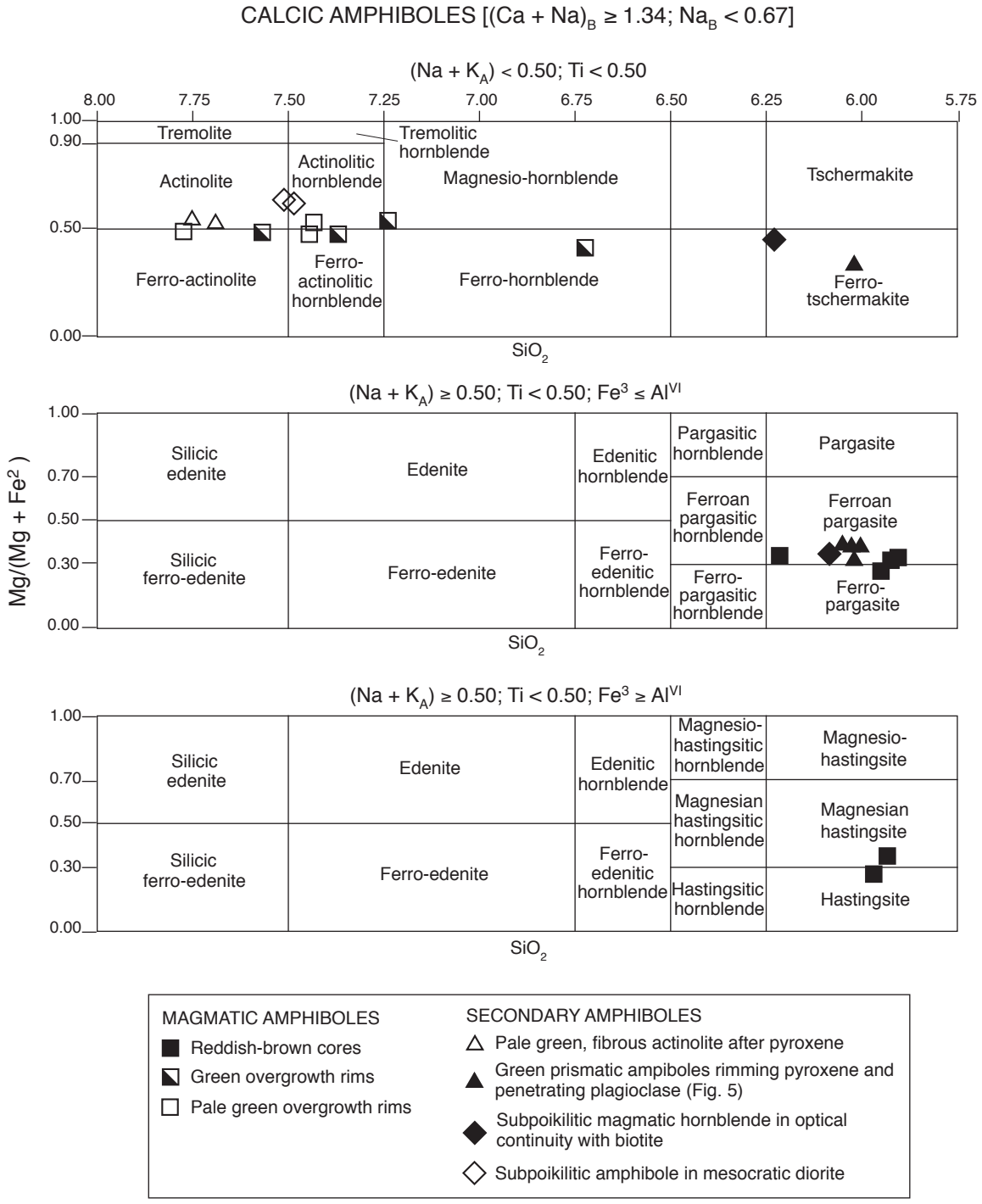

Figure 12. Amphibole compositional diagrams, using criteria of Leake (1978); modified from Leake and others (1987).

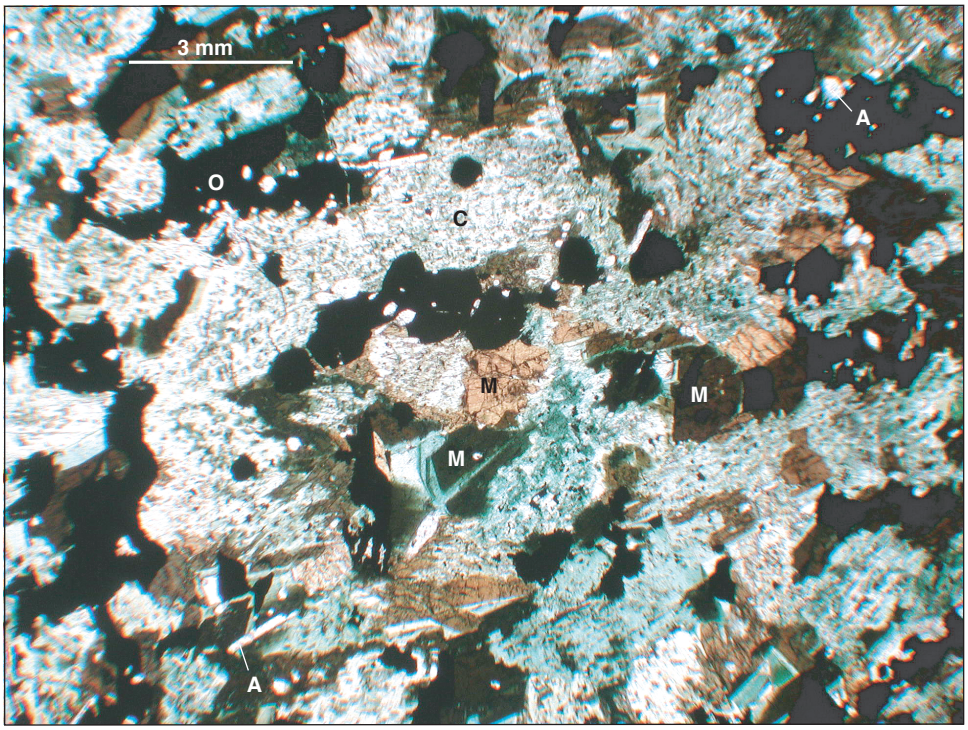

Figure 13. Photomicrograph of cumulate apatite-oxide-hornblende pyroxenite. Zoned amphibole in the center of the photograph is shown on Figure 14. C—clinopyroxene (augite); A—apatite; M—hornblende inferred to be a magmatic cumulate phase; O—Fe-Ti oxides. Photographed in plane-polarized light.

amphiboles increase gradationally in abundance from pyroxenite to hornblendite. In some cases the entire ferromagnesian component is composed of fine-grained felted mats of actinolite, but the precursor appears to have been composed of cumulate olivine, pyroxene, and oxides (Fig. 8).

Cumulate minerals in the pyroxenite include augite, magmatic hornblende, oxides, and apatite. Some samples contain abundant equant zones of fine-grained magnetite that are interpreted to be pseudomorphs of primary olivine (Fig. 8), similar to those in the melanocratic diorite. Semi-quantitative, energy-dispersive x-ray spectroscopy (EDS) analyses show that these dusty oxides in the pseudomorphs contain essentially no titanium, supporting the supposition that they are secondary products of what was most likely primary fayalitic olivine.

Augite forms subhedral to euhedral, equant cumulus grains of uniform size (Fig. 13). Alteration varies from rims and patchy replacement by dark green uralitic hornblende to complete replacement by optically continuous, colorless to green actinolite. Microprobe analyses of pyroxene show nearly ideal stoichiometric proportions of calcium (magnesium + iron) and silicon, with only minor substitution of aluminum, sodium, and titanium. Based on limited analyses, the pyroxene in hornblende pyroxenite is substantially less magnesian than pyroxene in the mesodiorite (Table 4).

Amphiboles in the pyroxenite and hornblendite apparently formed under a wide range of conditions that range from magmatic to deuteric. Magmatic hornblende forms blocky, reddish-brown grains with cores of deep red-brown ferroan pargasite to slightly magnesian hastingsite (Table 5B, samples HB-19-20 and HB-20-50). The cores are rimmed by rhythmic dark and pale green overgrowths that generally become more actinolitic toward the rim (Table 5B, samples HB-19-20 through HB-25-50; Figs. 12, 13, 14). Secondary actinolitic amphiboles range from green, optically continuous patches within augite grains (Fig. 14) to later patches composed of felted actinolite mats that have overprinted all other amphiboles, with the degree of replacement ranging from nil to 100 percent. The variable habits of actinolite, from magmatic overgrowth rims, to deuteric grains

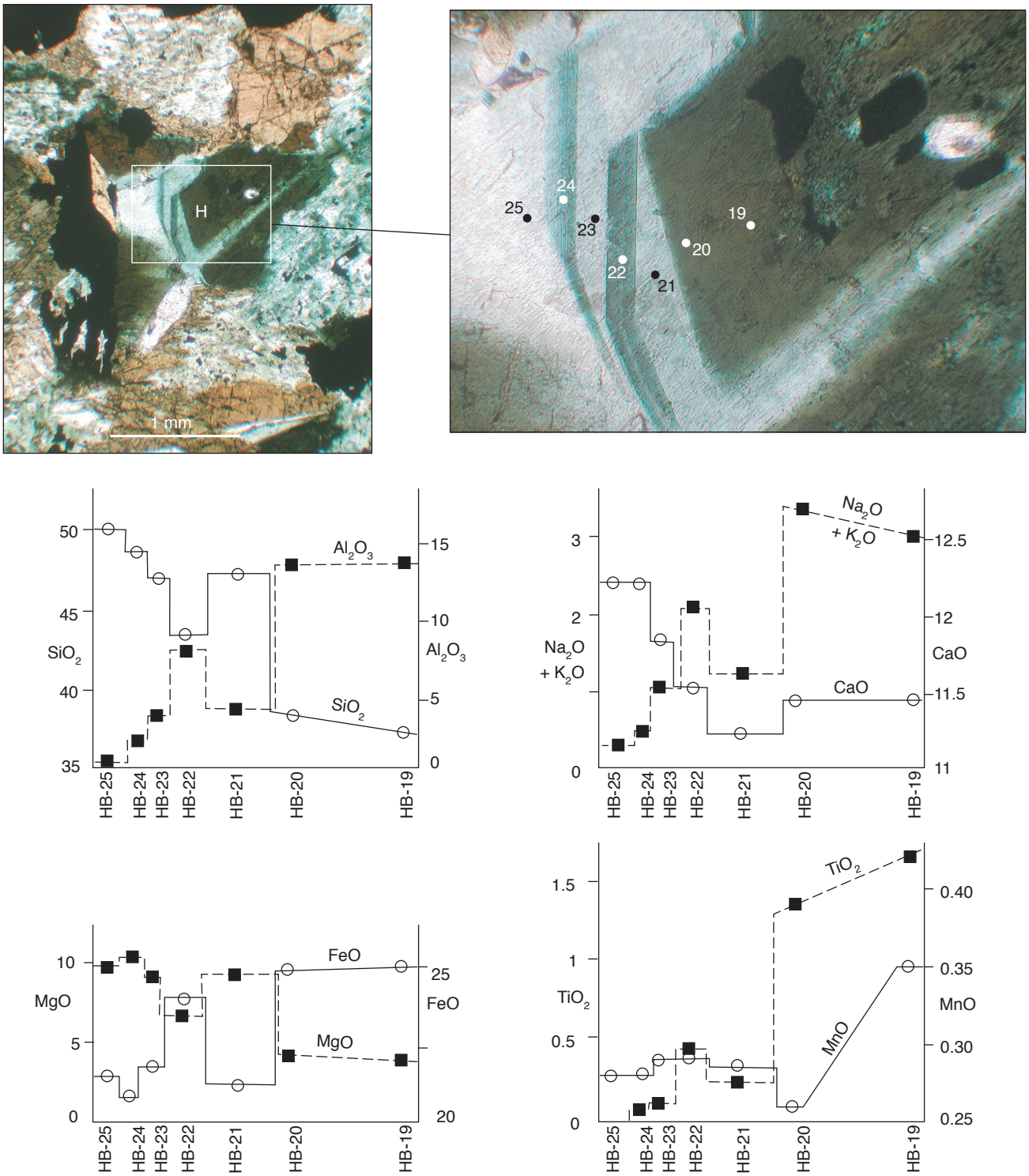

Figure 14. Chemical variation diagrams across zoned magmatic amphibole from drill core 6, 50- to 53-foot (15- to 16-meter) interval. Photomicrographs at the top show the amphibole and location of probe points. See Figure 12 and Table 5 for chemical composition and description of probed points.

confined within pyroxene precursors, to complete replacement by the felty actinolitic mats, implies a relatively water-rich magmatic environment in which volatiles were possibly increasingly concentrated as crystallization proceeded.

Oxide phases consist primarily of cumulus magnetite with abundant lamellae of exsolved ilmenite, and a lesser component of anhedral-interstitial grains of pure ilmenite. As in the diorite, magnetite is variably replaced by chlorite, biotite, or actinolite, leaving "thumbprints" of skeletal ilmenite surrounded by those silicate minerals. In other pseudomorphs, the oxide grains have a fine-grained dusty habit and irregular concentration that mimics olivine cracks and rims (Fig. 8).

Apatite is abundant, typically as prismatic crystals but also as larger 2- to 3-millimeter anhedral grains and locally optically continuous subpoikilitic masses (Fig. 8). There are minor amounts of anhedral-interstitial sphene and calcite (Table 6). Trace amounts of pyrite and chalcopyrite are also present as inclusions in oxide minerals, or associated with altered ilmenomagnetite grains. The only feldspar grain observed in the samples that were examined was a small, rounded inclusion within pyroxene.

Oxide-apatite rock (nelsonite)

The term nelsonite was first used for rutile-apatite rocks of igneous derivation from Nelson and Amherst Counties, Virginia, by Watson and Taber (1913), where the ideal cotectic ratio of oxides to apatite is approximately 2:1. Subsequently, the term has been expanded by others to include ilmenite- or magnetite-apatite rocks (Philpotts, 1967) of widely varying oxide:apatite ratios. Although some of the oxide-rich rocks from the Philbrook intrusion contain substantial apatite and could properly be termed nelsonite, most contain only a few percent apatite, and thus the term oxide rock is here used interchangeably with nelsonite.

Dense, metallic black, strongly magnetic, medium-grained and equigranular oxide rock/nelsonite comprises approximately 10 percent of the drill core. It occurs as steeply dipping, concentric layers at least 33 feet (10 meters) thick that seem to pinch out with depth (Fig. 4B). The proportion of apatite in the skeletonized core remnants varies considerably, from 2 to 30 percent. Minor anhedral-interstitial sphene and variable proportions of chlorite, amphibole, and/or clinopyroxene are present, and as the proportion of amphibole and/or pyroxene increases in modal volume, the rocks grade into hornblendite or pyroxenite, respectively. Minor amounts of pyrite and chalcopyrite occur in thin fractures, along with chlorite and calcite. Secondary blebs of sulfide occur within magnetite, and in some cases sulfides form discrete anhedral-interstitial blebs between grains of oxides.

Fe-Ti oxides occur mostly as 1- to 3-millimeter equant grains of magnetite with exsolved ilmenite lamellae along crystallographic planes, as well as a small amount of anhedral-interstitial ilmenite. Some magnetite has been selectively replaced by chlorite, producing ragged grains with protruding ilmenite lamellae. Traces of exsolved hematite rim lamellar ilmenite, and local finely exsolved grains of a darker gray phase, shown by microprobe analyses to be an aluminum-bearing phase such as hercynite ($FeAl_2O_4$), impart a woven appearance to the magnetite. The later-crystallized interstitial ilmenite and the exsolved lamellar ilmenite are chemically similar; the magnetite is very pure except where it contains exsolved hercynite, in which case it contains appreciable aluminum and increased titanium (Table 8).

Apatite crystals have smooth and rounded common boundaries with oxides, and rarely form large, subpoikilitic grains. Apatite from nelsonite is compositionally indistinguishable from apatite in the meladiorite, with the exception of a slightly less negative europium anomaly (Fig. 9; Table 7).

Chlorite is the third most common component of the nelsonite, and forms lobate masses of secondary origin that are possibly after pyroxene or hornblende. However, the lack of oxide, sphene, and epidote scraps normally associated with secondary chlorite implies that the alteration by-products were transported away by deuteric fluids and redeposited elsewhere. Pyroxene and hornblende, where present, are similar in morphology to that in the pyroxenite and hornblendite.

Crystallization sequence

Limited outcrop data and drill core preclude elucidation of a well-ordered crystallization history. Cumulate textures and cumulate foliation are common, and evidence for modal layering (Fig. 6) and from drilling data implies that the Philbrook intrusion is a magmatically layered, mafic igneous body. All rock types are interpreted to be comagmatic products of an iron- and phosphorous-enriched magma. Based on a suite of 25 samples of mesodiorite and meladiorite collected from outcrops of the Philbrook intrusion for geochemical analyses, Geary (2012) suggested that the Philbrook intrusion follows evolutionary trends of rocks associated elsewhere with anorthosite massifs. He suggested that at Philbrook the mesocratic diorite was the first phase to crystallize, followed by melanocratic diorite, pyroxenite, and nelsonite;

Table 8. Micropbrobe analyses of oxides. Drill-hole locations are shown on Figure 4B.

	Weight percent oxides								Number of ions based on 12(O) in formula					
Sample	SiO_2	TiO_2	Al_2O_3	FeO	MnO	CaO	Total	Cation sum	Si	Ti	Al	Fe	Mn	Ca
3-136-LI1	0.33	50.45	0.00	45.77	2.22	0.21	98.98	6.17	0.033867149	3.893868615	0	3.928448303	0.192987283	0.023092885
3-136-MG1	0.49	0.47	0.08	92.09	0.04	0.23	93.4	9.11	0.074311883	0.053606255	0.014303415	11.68019488	0.005138463	0.03737526
3-136-LI2	0.56	50.95	0.03	46.15	2.11	0.2	100	6.09	0.056753642	3.883339153	0.003584384	3.911585661	0.181133669	0.021718504
3-136-MG2	0.5	0.96	0.06	92.57	0.05	0.22	94.36	8.99	0.074769318	0.107964274	0.010577724	11.57708196	0.006333364	0.035250907
9-52-C1	0.47	50.29	0.04	45.65	1.54	0.22	98.21	6.20	0.048465307	3.900049962	0.004862736	3.936854133	0.134513183	0.024308043
6-52-LI3	0.42	49.89	0.00	45.17	1.58	0.22	97.28	6.26	0.043737865	3.907304184	0	3.933995111	0.139372279	0.024548512
5-52-MG3	0.57	16.88	5.92	72.08	0.51	0.22	96.18	7.36	0.069832482	1.555286811	0.855050764	7.385379756	0.05292536	0.028880154
8-52-LI4	0.46	50.51	0.05	44.73	1.51	0.2	97.46	6.22	0.047633745	3.933595374	0.006103999	3.873746716	0.132447833	0.022191215
7-52-MG4	0.3	3.43	4.57	84.83	0.13	0.22	93.48	8.47	0.042287232	0.363611452	0.759437047	10.0002972	0.015521811	0.033228053

Drill hole 3, 136' depth

3-136-LI1 and 2—Exsolved lamellar ilmenite in magnetite
3-136-MG1 and 2—Magnetite host to respective lamellar ilmenite numbers above

Drill hole 1, 52' depth

9-52-C1—Interstitial composite ilmenite
6-52-LI3 and 8-52-LI4—Exsolved lamellar ilmenite in magnetite
5-52-MG3 and 7-52-MG4—Magnetite host to respective ilmenite numbers above

Figure 15. Photomicrograph of sericite-altered, cumulate-foliated anorthosite. Photographed in cross-polarized light.

consistent with a suggestion by Ashwal (1993) that rocks associated with massif anorthosites evolve along a trend of decreasing SiO_2 and Al_2O_3 and increasing MgO and FeO. The minor anorthosite at Philbrook is of unknown timing due to lack of exposure. Although it may have originated as a strongly foliated, plagioclase-rich cumulate layer (Fig. 15) now included within the mesodiorite, the fact that it occurs as xenoliths coupled with the positive europium anomaly (Fig. 11) indicates that it is more likely an inclusion carried up from a magma chamber at depth.

A volatile-enriched magma is supported by the following evidence: 1. Ubiquitous deuteric alteration of pyroxene to amphibole; 2. Reaction rims of ferroan pargasite between pyroxene and plagioclase (possibly a liquid reaction); 3. Cumulus magmatic hornblende; 4. Alteration of magnetite to hydrous assemblages of biotite, chlorite, and amphibole; 5. Patchy alteration of feldspars to sericite-calcite-epidote-chlorite; and 6. Late-stage pegmatite and volatile-rich net-veining features in the diorite. A wet magma is consistent with the highly fractionated and incompatible element-enriched nature of the magma, and with a high oxygen fugacity to aid crystallization of magnetite. Although normal differentiation processes are probably responsible for much of the observed rock variations, late-stage deuteric alteration has obscured much of the primary textures and lithologies.

POSSIBLE ANALOGUES TO THE PHILBROOK INTRUSION

Oxide ± apatite-rich rocks of magmatic origin occur in a variety of intrusive settings, but the Philbrook intrusion bears some similarity to Fe-rich dioritic to gabbroic and noritic rocks associated with Proterozoic massif-type anorthosites, collectively termed the "AMCG suite" (A—Anorthosite; M—Mangerite [orthopyroxene-bearing monzonite], C—Charnockite [orthopyroxene-bearing granite], G—Granite). Also associated with the AMCG suite are rapakivi-textured granites and small volumes of Fe-Ti oxide ores. Most AMCG suites are younger than the Philbrook intrusion (approximately 1,000 to 1,650 Ma). Massif-type anorthosites are well-known throughout the world, mainly in the northern hemisphere, where their distribution closely follows orogenic belts (for example McLelland and others, 2010). AMCG suites typically occur in high-grade Proterozoic metamorphic terranes, and some, such as the Laramie complex of Wyoming, were emplaced

into Archean crust or at the boundary between Archean and Proterozoic terranes (for example Mitchell and others, 1996). Most scientists have postulated deep or mid-upper crustal (6.2 to 9.3 miles [10 to 15 kilometers]) depths of emplacement for these anorthosite suites (Ashwal, 1993).

Although no anorthosite massif has been identified at Philbrook, there are at least some anorthositic components, and the chemistry of the dioritic phases resembles that of mafic-intermediate composition rocks elsewhere associated with massif-type anorthosite bodies. Using a $CaO - Na_2O + K_2O - Fe_2O_3t$ triangular diagram, Geary (2012) showed that samples of Philbrook-intrusion mesodiorite plot within the compositional fields of anorthosite massif-related leucogabbro and gabbro, and Philbrook-intrusion meladiorite plots within the field of oxide gabbronorite and oxide-apatite gabbronorite (Fig. 16A). Speculatively, the compositional similarities of these phases of the Philbrook intrusion to compositions of rocks related to massif-type anorthosites implies that the Philbrook intrusion may have undergone a similar chemical evolution. Trace elements in the Philbrook-intrusion mesocratic and melanocratic diorites also closely match those of rocks related to anorthosite massifs (Fig. 16B), except that Philbrook-intrusion rocks show elevated barium and thorium values, possibly attributable to a higher degree of interaction with an enriched mantle or upper crust prior to emplacement (Geary, 2012).

In a highly speculative scenario, the Philbrook intrusion may represent a differentiate from an as-yet unidentified anorthosite body at depth that was subsequently injected upward to form a funnel-shaped intrusion. Upon reaching a higher level in the crust, the diorite fractionally crystallized to form the oxide-rich and melanocratic layers. The bulk composition of the intrusion may be the melanocratic ferrodiorite, which could produce an Fe-Ti-P rich fraction that split immiscibly to form the nelsonite phases. However, the abundance of cumulate textures in all the phases of the Philbrook intrusion implies that crystal fractionation was most likely responsible for the layering and variations in the abundance of oxide minerals and apatite.

CONCLUSIONS

- The Philbrook intrusion is likely a funnel-shaped intrusion with steep walls. The extent of the pluton is delineated by a pronounced positive aeromagnetic signature, by which the pluton is estimated to be approximately 2 mi^2 (5 km^2) in surface area.
- Hornblende that is inferred to be of magmatic origin, based on petrographic textural evidence, yields an $^{40}Ar/^{39}Ar$ age of 1,854 ± 4 Ma. Although this age is similar to metamorphic ages obtained within the nearby Paleoproterozoic Mille Lacs Group and Cuyuna North Range, and it cannot be ruled out that the 1,854 Ma age instead reflects a Penokean metamorphic overprint, the presence of delicate magmatic overgrowth rims on hornblende crystals imply that the age most likely represents primary crystallization.
- The intrusion was emplaced into upper greenschist/lower amphibolite grade Archean and/or Paleoproterozoic metasedimentary rocks that may have been hydrothermally altered by the Philbrook intrusion. Alternatively, the country rocks were hydrothermally altered prior to emplacement of the Philbrook pluton, in which case they may have supplied the hydrous fluids responsible for the pervasive deuteric alteration in the pluton.
- Melanocratic, apatite- and oxide-rich diorite is the predominant rock type in the intrusion, along with a subordinate amount of mesocratic diorite that bears inclusions or segregations of anorthosite. Based on contoured magnetic data, drill records, and available drill core, the ultramafic rock types (pyroxenite, hornblendite, and oxide-apatite rocks) comprise a substantial proportion of the intrusion, and occupy a concentric layer within it; however, the geometry of this layering is poorly constrained.
- Amphiboles of various types and habit are abundant and in many cases have obliterated the primary rock textures, and some or all of the rocks classified as hornblendite may be composed entirely of secondary amphiboles that formed by deuteric processes, implying that the intrusion cooled from a hydrous magma. However, with the exception of phases completely replaced by felty actinolitic amphibole, all of the various phases exhibit relict cumulate textures.
- The origin of the pluton remains enigmatic; however, it is postulated that it may be similar to iron-rich mafic rocks and oxide-apatite rocks elsewhere associated with large anorthosite massifs.
- At present, the oxide concentrations in this pluton are uneconomic. However, given the minimal thickness of glacial overburden and apparent internal layering, this intrusion could make an attractive site for a small-scale exploration program. To date, no analyses have been obtained

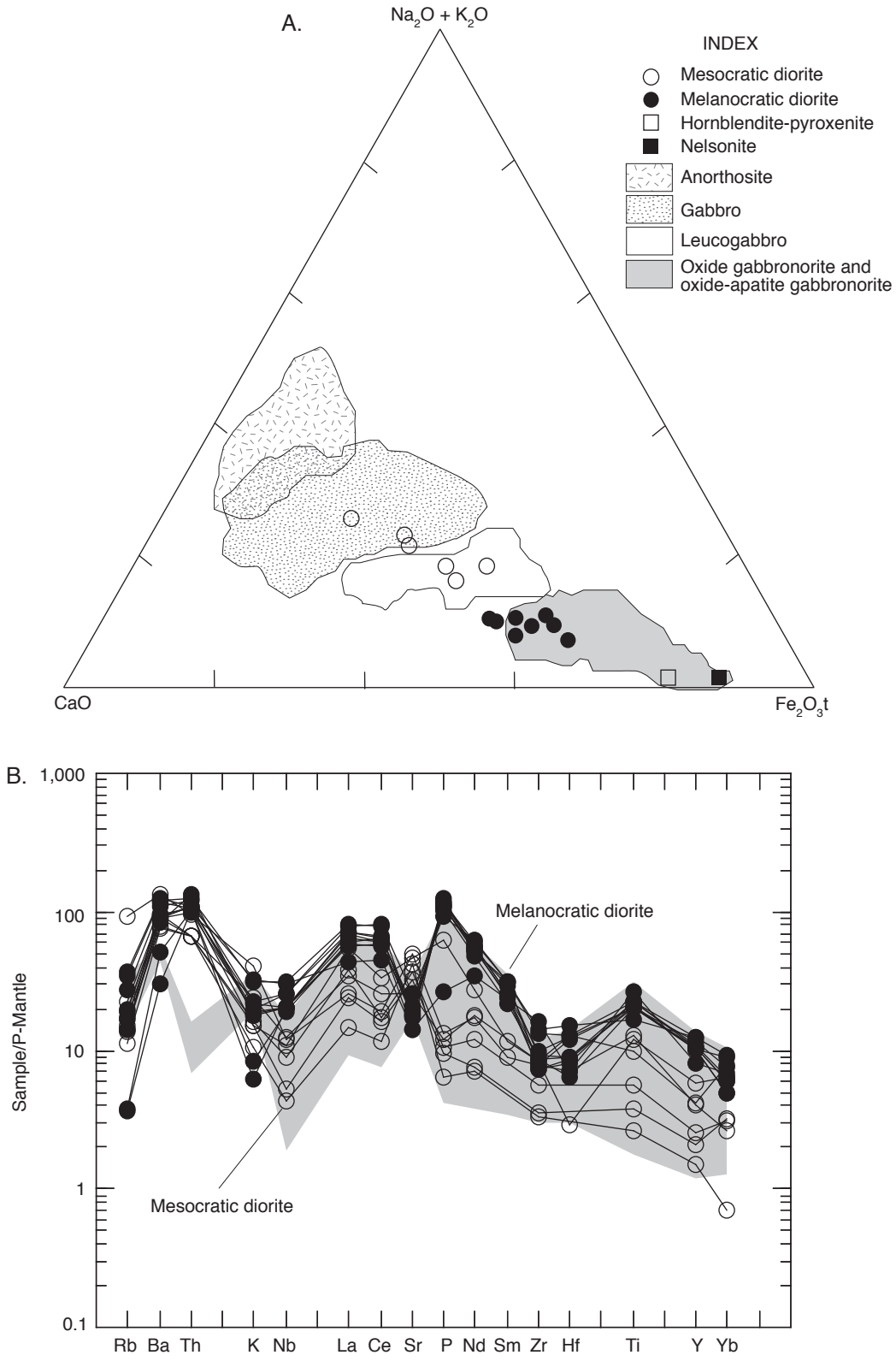

Figure 16. A. Compositional variation diagrams of rocks from the Philbrook intrusion compared to anorthosite-suite related rocks from the Adirondack, Harp Lake (Labrador), and Morin (Quebec) massifs (Ashwal, 1993; Seifert and others, 2010).

B. Trace-element variation diagram of samples of Philbrook-intrusion meladiorite and mesodiorite compared to the Adirondack anorthosite suite (shaded field).

for any of the platinum-group elements, but these elements should be considered in any future exploratory work.

ACKNOWLEDGEMENTS

D.L. Southwick and G.B. Morey, formerly of the Minnesota Geological Survey, provided advice and insight at the time Boerboom's (1987) thesis was in progress, and the Minnesota Geological Survey provided financial assistance for analytical work and thin-section preparation during that study.

REFERENCES

Ashwal, L.D., 1993, Anorthosites: New York, Springer-Verlag, 422 p.

Boerboom, T.J., 1987, Tourmalinites, nelsonites, and related rocks (Early Proterozoic) near Philbrook, Todd County, Minnesota: Duluth, Minn., University of Minnesota Duluth, M.S. thesis, 212 p.

———1989, Tourmaline in Early Proterozoic metasedimentary rocks near Philbrook, northeastern Todd County, central Minnesota: Minnesota Geological Survey Report of Investigations RI-38, 25 p.

———2007, Bedrock geology, pl. 2 *of* Setterholm, D.R., project manager, Geologic atlas of Todd County, Minnesota: Minnesota Geological Survey County Atlas C-18, pt. A, scale 1:200,000.

Boerboom, T.J., and Holm, D.K., 2000, Paleoproterozoic intrusive igneous rocks of southeastern Stearns County, central Minnesota: Minnesota Geological Survey Report of Investigations RI-56, 36 p.

Boerboom, T.J., Setterholm, D.R., and Chandler, V.W., 1995, Bedrock geology, pl. 2 *of* Meyer, G.N., project manager, Geologic atlas of Stearns County, Minnesota: Minnesota Geological Survey County Atlas C-10, pt. A, 7 pls., scales 1:100,000 and 1:200,000.

Cade, P.A., 1987, Magnetic and gravity survey over a buried Precambrian mafic body, Todd County, Minnesota: Bowling Green, Ohio, Bowling Green State University, M.S. thesis, 115 p.

Geary, J., 2012, geochemistry of Fe-Ti oxide-rich diorites: Philbrook, Minnesota: St. Paul, Minn., Macalester College, senior thesis, 23 p.

Grout, F.F., and Wolff, J.F., Sr., 1955, The geology of the Cuyuna District, Minnesota: A progress report: Minnesota Geological Survey Bulletin 36, 144 p.

Holm, D.K., Schneider, D.A., Rose, S., Mancuso, C., Mckenzie, M., Foland, K.A., and Hodges, K.V., 2007, Proterozoic metamorphism and cooling in the southern Lake Superior region, North America and its bearing on crustal evolution: Precambrian Research, v. 157, p. 106-126.

Holm, D.K., Van Schmus, W.R., MacNeill, L.C., Boerboom, T.J., Schweitzer, D., and Schneider, D., 2005, U-Pb zircon geochronology of Paleoproterozoic plutons from the northern mid-continent, U.S.A.: Evidence for subduction flip and continued convergence after geon 18 Penokean orogenesis: Geological Society of America Bulletin, v. 117, nos. 3/4, p. 259-275.

Jirsa, M.A., Boerboom, T.J., Chandler, V.W., Mossler, J.H., Runkel, A.C., and Setterholm, D.R., 2011, Geologic map of Minnesota—Bedrock geology: Minnesota Geological Survey State Map S-21, scale 1:500,000.

Jirsa, M.A., Chandler, V.W., Lively, R.S., and Boerboom, T.J., 2003, Maps of bedrock geology and superimposed magnetic on gravity (SMOG) anomaly for east-central Minnesota: Minnesota Geological Survey Miscellaneous Map M-132, scale 1:200,000.

Jirsa, M.A., Miller, J.D., Jr., and Severson, M.J., 2006, Geology, geochemistry, and PGE potential of mafic-ultramafic intrusions in Minnesota, excluding the Duluth Complex: Minnesota Geological Survey Open-File Report OFR 06-1, 13 p.

Leake, B.E., 1978, Nomenclature of amphiboles: Final report by the subcommittee on the amphibole group, as approved by the International Mineralogical Association Commission on new minerals and mineral names: American Mineralogist, v. 63, p. 1023-1052.

McLelland, J.M., Selleck, B.W., Hamilton, M.A., and Bickford, M.E., 2010, Late- to post-tectonic setting of some major Proterozoic anorthosite-mangerite-charnockite-granite (AMCG) suites: The Canadian Mineralogist, v. 48, p. 729-750.

Mitchell, J.N., Scoates, J.S., Frost, C.D., and Kolker, A., 1996, The geochemical evolution of anorthosite residual magmas in the Laramie Anorthosite Complex, Wyoming: Journal of Petrology, v. 57, no. 5, p. 637-660.

Morse, S.A., 1979, Kiglapait geochemistry; II, Petrography: Journal of Petrology, v. 20, no. 3, p. 591-624.

Philpotts, A.R., 1967, Origin of certain iron-titanium oxide and apatite rocks: Economic Geology, v. 62, no. 3, p. 303-314.

Schneider, D.A., Holm, D.K., O'Boyle, C., Hamilton, M., and Jercinovic, M., 2004, Paleoproterozoic development of a gneiss dome corridor in the southern Lake Superior region, USA, *in* Whitney, D.L., Teyssier, C., and Siddoway, C.S., eds., Gneiss domes in orogeny: Geological Society of America Special Paper 380, p. 339-357.

Schulz, K.A., and Cannon, W.E., 2007, The Penokean Orogeny in the Lake Superior region: Precambrian Research, v. 157, p. 4-25.

Seifert, K.E., Dymek, R.F., Whitney, P.R., and Haskin, L.A., 2010, Geochemistry of massif anorthosite and associated rocks, Adirondack Mountains, New York: Geosphere, v. 6, no. 6, p. 855-899.

Southwick D.L., 1994, Assorted geochronologic studies of Precambrian terranes in Minnesota: A potpourri of timely information, *in* Southwick, D.L., ed., Short contributions to the geology of Minnesota: Minnesota Geological Survey Report of Investigations RI-43, p. 1-19.

Southwick, D.L., Morey, G.B., and McSwiggen, P.L., 1988, Geologic map (scale 1:250,000) of the Penokean Orogen, central and eastern Minnesota, and accompanying text: Minnesota Geological Survey Report of Investigations RI-37, 25 p.

Southwick, D.L., Setterholm, D.R., and Boerboom, T.J., 1990, Scientific test drilling in west-central Minnesota: Summary of lithologic and stratigraphic results, 1987-1988, and some preliminary geologic conclusions: Minnesota Geological Survey Information Circular IC-31, 98 p.

Sun, S., and McDonough, W.F., 1989, Chemical isotopic systematics of oceanic basalts: Implications for mantle composition and processes, *in* Saunders, A.D., and Norry, M.J., eds., Magmatism in the ocean basins: Geological Society of London Special Publication, v. 42, p. 313-345.

Streckeisen, A.L., 1973, Plutonic rocks—Classification and nomenclature recommended by the IUGS subcommission on the systematics of igneous rocks: Geotimes, v. 18, no. 10, p. 26-30.

Taylor, S.R., and McClennan, S.M., 1985, The continental crust: Its composition and evolution: Oxford, Blackwell Scientific, 312 p.

Thiel, G.A., 1926, Phosphorous iron ores on the Cuyuna Range: Engineering and Mining Journal, v. 121, p. 687-690.

Upham, W., 1888, The geology of Wadena and Todd Counties, chapter 11 *of* Winchell, N.H., and Upham, W., Geology of Minnesota: Geological and Natural History Survey of Minnesota Final Report, v. 2, p. 562-579.

Vallini, D.A., Cannon, W.F., Schulz, K.J., and McNaughton, N.J., 2007, Thermal history of low metamorphic grade Paleoproterozoic sedimentary rocks of the Penokean Orogen, Lake Superior region: Evidence for a widespread 1,786 Ma overprint based on xenotime geochronology: Precambrian Research, v. 157, p. 169-187.

Watson, T.L., and Taber, S., 1913, Geology of the titanium and apatite deposits of Virginia: Virginia Geological Survey Bulletin, v. 3a, 308 p.

APPENDIX

SAMPLE LOCATIONS

Samples from outcrop located by 7.5' topographic maps

PB-1-OC—Apatite-rich melanocratic diorite outcrop, T. 133 N., R. 32 W., sec. 34, BCDA
PB-OC-PG—Coarse-grained mesocratic diorite, outcrop sample, T. 133 N., R. 32 W., sec. 34, BACD

Samples from drill cores in T. 132 N., R. 32 W., sec. 3, BB (Fig. 4B)

PB-1-74—Oxide-rich hornblende pyroxenite; drill hole 1, 74' depth
PB-5-179—Oxide rock; drill hole 5, 179' depth
PB-1-57—Hornblende and pyroxene-bearing apatitic oxide rock; estimated 88% oxide, 2% apatite, 10% silicates
PB-3-72—Oxide-rich hornblendite; 92% oxide, 5% chlorite/actinolite, 3% apatite
PB-3-132—Oxide-rich hornblendite; 50% oxide, 10% apatite, 40% silicates
PB-5-208—Oxide-apatite rock; 10-15% apatite
PB-8-55—Oxide- and apatite-bearing pyroxenite
PBI-2-88—Oxide-apatite-rich melanocratic diorite; drill core PBI-88-2
PBI-88-1-23—Oxide-apatite-rich melanocratic diorite; drill core PBI-88-1

Samples collected by Jesse Geary, Macalester College; UTM coordinates WGS 1984 (equivalent to nad 1983 zone 15)

Sample		UTM easting	UTM northing
PB01	Meladiorite	369119mE	5126481mN
PB02	Meladiorite	369793mE	5126231mN
PB05	Meladiorite	368003mE	5126866mN
PB06	Meladiorite	369034mE	5127547mN
PB08	Meladiorite	369092mE	5127808mN
PB09	Meladiorite	368888mE	5127399mN
PB10	Meladiorite	368720mE	5127392mN
PB11	Meladiorite	497981mE	4961884mN
PB12	Intermediate between meladiorite and mesodiorite	368262mE	5127663mN
PB13	Intermediate between meladiorite and mesodiorite	368212mE	5127827mN
PB14	Intermediate between meladiorite and mesodiorite	368238mE	5127858mN
PB15	Mesodiorite	368251mE	5127949mN
PB16	Mesodiorite	368244mE	5127955mN
PB17	Mesodiorite	368267mE	5127955mN
PB18	Mesodiorite	368307mE	5127952mN
PB20	Mesodiorite	368574mE	5128218mN